REAR AXLE GEAR WHINE NOISE ABATEMENT VIA ACTIVE VIBRATION CONTROL OF THE REAR SUBFRAME

Thesis

Submitted to

The School of Engineering of the

UNIVERSITY OF DAYTON

In Partial Fulfillment of the Requirement for

The Degree of

Master of Science in Mechanical Engineering

By

Jie Deng

UNIVERSITY OF DAYTON

Dayton, Ohio

December, 2015

REAR AXLE GEAR WHINE NOISE ABATEMENT VIA ACTIVE VIBRATION CONTROL OF THE REAR SUBFRAME

Name: Deng, Jie

APPROVED BY:

Reza Kashani, Ph.D.
Advisory Committee Chairman
Professor
Department of Mechanical and Aerospace Engineering

Dave Myszka, Ph.D.
Committee Member
Associate Professor
Department of Mechanical and Aerospace Engineering

David Perkins, Ph.D.
Committee Member
Lecturer
Department of Mechanical and Aerospace Engineering

John G. Weber, Ph.D.
Associate Dean
School of Engineering

Eddy M. Rojas, Ph.D., M.A., P.E.
Dean, School of Engineering

ABSTRACT

REAR AXLE GEAR WHINE NOISE ABATEMENT VIA ACTIVE VIBRATION CONTROL OF THE REAR SUBFRAME

Name: Deng, Jie
University of Dayton

Advisor: Dr. Reza Kashani

An active, feedback vibration control strategy with the goal of abating gear whine noise in rear- wheel and all-wheel drive vehicles is developed. The control strategy was implemented using two small inertial (proof mass) actuators, mounted on the rear subframe of a luxury all-wheel drive sedan with independent rear suspension, as the active elements in this application. Acceleration information measured by accelerometers nearly-collocated with the actuators was used as the feedback signal.

The effectiveness of active vibration control was successfully demonstrated by examining the extent of reduction in the shaker induced vibration of the rear subframe as well as the sound pressure inside the vehicle. The evaluation of the active control scheme was extended to rolling dynamometer tests, during which effective reduction of vibration of rear subframe and the pressure inside the vehicle were demonstrated.

ACKNOWLEDGMENTS

My special thanks are in order to Dr. Reza Kashani, my advisor, for providing the time and equipment necessary for the work contained herein, and for directing this thesis and bringing it to its conclusion with patience and expertise. In addition, the financial and technical support of Fiat Chrysler Corporation is greatly appreciated.

I would also like to express my appreciation to everyone who has helped me with this work. This includes my committee member Dr. Dave Myszka and Dr. David Perkins, for giving suggestions on this thesis; Tianyang Chen, who offered guidance with simulation; Jordan Francis, for providing hands-on help on the test vehicle; Larry Collins, who aided in the setup of the experiment; Mechanical and Aerospace Engineering department staff member Ms. Ginger Stuck, for her administrative help.

TABLE OF CONTENTS

LIST OF ILLUSTRATIONS

CHAPTER I

INTRODUCTION

1.1 Problem Statement

Rear axle gear whine noise is caused mainly by the gear mesh vibration in the powertrain. This vibration is in turn transmitted thru the rear axle gear housing, the corresponding subframe, as well as other support structures to the vehicle cabin as an unpleasant tonal noise [1, 2]. Although gear mesh forced vibration transmits into the cabin at all speeds, but at certain speeds/frequencies the transmission of vibration is more dominant than others. This is due to the matching of the gear mesh frequency with one (or multiple) resonant frequency (ies) of a structural element along the transmission path (consisting of the drive shaft, rear differential, rear subframe, and the vehicle body).

1.2 Vibration Control Strategies

1.2.1 Passive Vibration Control

Passive vibration control is a strategy utilizing a device which does not need any power consumption. Two types of such devices are used in the passive vibration control: broadband [3] and tuned devices. Viscous and viscoelastic dampers are examples of broadband passive vibration control devices. As to the passive tuned devices, tuned mass damper (TMD) and dynamic absorber (DA) are two of the most commonly used devices

in tuned vibration control [4]. The makeup of these two devices consists of a mass, a spring, and a damper with decent amount of damping in TMD but negligible amount of damping in DA. Passive tuned devices are simple, low cost and stable but are not adjustable when the parameters of the controlled structure are changed.

1.2.2 Active Vibration Control

Active vibration control uses an actuation device (actuator) to generate force moment exerted on the controlled structure to fulfill the goal of vibration reduction. A sensor[1] is also used, in conjunction with the actuator to provide information on the vibration of the structure. The readings from the sensor are manipulated in the actuator to do the appropriate action on the structure. This kind of control strategy is powerful and exact especially in the areas where high precision control is needed. It can coordinate itself with the varying parameters of the structure and always keep its most optimal effectiveness. However, active vibration control systems come with high cost and complexity and are prone to instability. Moreover, They consume energy and require periodic maintenance.

The heart of an active vibration control application is the actuator which can be classified as „regular actuator" and „proof mass actuator (PMA)". A regular actuator gets attached to the structure being controlled at one end and to an anchor point at the other. A proof mass actuator uses a moving mass (called proof mass) as its anchor and uses its inertia force of the proof mass as its actuation force. Figure 1.1 shows the schematic diagram of a regular actuator and a PMA actuating a structure. A shown in Figure 1.1 is a

[1] Some actuators will have a sensor inside since manufactured to pursue a better control effectiveness for this collocated arrangement in certain control scenarios [5].

regular actuator consists of only an active actuation element while a PMA contains an active actuation element and a proof mass attached to it.

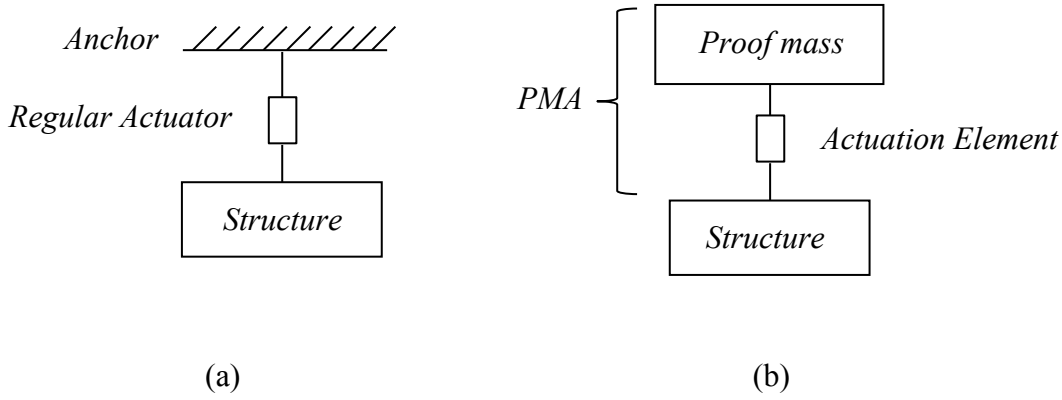

(a) (b)

Figure 1.1: Schematic diagram of a regular actuator (a) and a PMA (b) appended to a structure

1.3 Active Vibration Control to Abate Gear Whine Noise

In this research project active vibration control was applied to the rear subframe of an all-wheel drive sedan to abate the gear whine noise in the cabin. Proof mass actuators (PMAs) were used in this active vibration control application. As stated earlier, these actuators generate their force by pushing against a suspended mass and thus do not need their other ends to be anchored. Chapter 2 describes the inner working of these actuators and how they can be used in active vibration control applications.

With proof mass actuators (PMAs) as the actuation mechanism, the following two active vibration control strategies, each with its own advantages and disadvantages, were considered in this work:

1. Set natural frequency of the PMA substantially lower than the natural frequency of the structure targeted for damping/absorption.

This strategy results in proof mass actuator possessing no unwanted dynamics over the frequencies they are intended to function. This allows treating the proof mass actuator the same way as an anchored actuator which in turn enables the control designer to use traditional and familiar active control schemes.

2. Place the natural frequency of the PMA within its operating frequency range (bandwidth).

This strategy results in a proof mass actuator with a natural frequency (and the associated phase angle) in the frequency range where the active system needs to be most effective, making the synthesis of active control strategy somewhat more involved/elaborate. The advantage of such strategy is lower power consumption of the actuator.

Both strategies can be used in the active whine noise control application, depending on the character of the noise.

It is more straightforward to use the strategy 1 in vibration control as long as the actuator does not overheat because of the large power consumption. No phase angle issue needs to be considered during the control process. The control scheme for the strategy 2, on the other hand, is more involved.

1.4 Literature Survey

The two above-mentioned active feedback control strategies with the goal of abating gear whine noise in rear-wheel and all-wheel drive vehicles were experimented with aiming to absorb the vibration somewhere along its transmission path to the test

vehicle cabin, but preferably as close as possible to the source of vibration, i.e., the rear differential.

Following to the synthesis and numerical simulation of the two active vibration control strategies, they were both successfully tested on a simple structure, i.e., a beam, in the laboratory. One of the active vibration control strategies has been implemented on an all-wheel drive test vehicle exhibiting whine noise at around 450Hz. The effectiveness of active acoustic damping system was evaluated objectively and subjectively using rolling dynamometer tests. The active control scheme absorbed an appreciable amount of vibration of the rear axle and the corresponding whine noise.

Isao Nishimura, et al., [7] proposed a control algorithm applied in active TMD control. The active TMD is a system by adding a regular actuator in a passive TMD with one end fixed on the structure and the other end attached to the mass of the TMD. They measured the relative velocity between the structure and the TMD as well as the acceleration of the structure, then fed the two signals back thru two optimal gains, to the actuator. The enhanced effectiveness of the active TMD over the passive TMD is greatly distinguishable, proving the feasibility of this control scheme in active TMD control.

One of the approaches to implement the control strategy 2 is the estimator-based control schemes such as Linear Gaussian Regulation (LQG) commonly used in active multi resonance damping [8]. Before carrying out this sort of control, the model of the structure including with first few modes of the structure needs to be constructed. In the absence of measured states, a Kalman estimator is designed to estimate the states. The estimated states are feedback to an optimal Linear Quadratic Regulator (LQR) to generate

the control force. The Schematic diagram of a plant and a Kalman estimator is shown in Figure 1.2, where the *Ke* is the Kalman estimator gain.

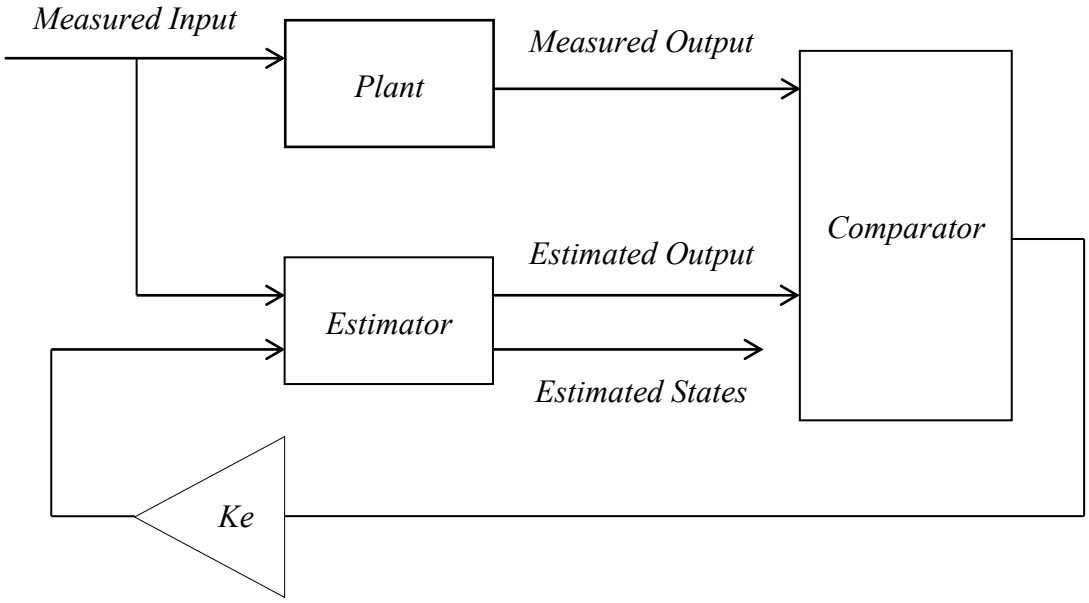

Figure 1.2: Schematic diagram of a plant and a Kalman estimator

Chin-Hsiung Loh, et al., [9] presented a prediction-type Kalman filter approach used for estimating the full-state variables of a six-story eccentric building subject to seismic perturbation, from a limited number of measurements. The building equipped with a dual tuned mass damping system is subjected to a full-state feedback control strategy for the control of its bending-torsion motion. They used the measurement signals of the 2nd and 6th floors to control the structural response and found that using the Kalman filter technique to predict the full state for control will have a similar control effectiveness as optimal full-state feedback control (LQR).

The organization of the thesis is as follows: chapter 2 discusses the mechanics of PMAs and how they can be used in vibration control applications. The development of

the aforementioned two control strategies as well as their laboratory applications on test structures are discussed in chapter 3. The implementation of one of the control schemes on the test vehicle along with the measured results showing its effectiveness in abating gear whine vibration and noise are presented in chapter 4. A summary of the work as well as some recommendation for future work are presented in chapter 5.

CHAPTER II

PROOF MASS ACTUATOR INTRODUCTION

2.1 Proof Mass Actuator

Proof mass (also known as inertial) actuators are used for actively abating the gear whine noise. To actuate these actuators do not need to push/pull against an anchor; A proof mass actuator (PMA) is comprised of parallel arrangement of spring and an active element pushing/pulling against a mass (known as proof mass or inertial mass). Figure 2.1 shows the schematic of such actuator appended to a structure. The force of such actuator is the reaction force caused by the acceleration of the suspended mass.

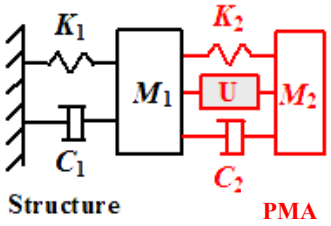

Figure 2.1: Schematic of a PMA installed on a structure

Depending on the application, some damping is incorporated into the makeup of PMA. Thus a proof mass actuator can be viewed as a spring mass damper system with an

active element in parallel with its spring-damper suspension. Depending on the application, the active element could be piezoelectric, electromagnetic, magnetostrictive, or even hydraulic/pneumatic. Piezoelectric and electromagnetic actuators are the two types of PMAs used in this project.

2.2 Piezoelectric and Electromagnetic PMAs Comparison

The piezoelectric actuator is the actuator using piezoelectric materials as active material in which application of a voltage to the material causes it to expand. It has extremely fine positioning resolution, but a short limited motion. The makeup of an electromagnetic actuator consists of a coil wound an iron core called an armature, placed in a magnetic field. The armature will move back and forth when alternating current flows through the coil. It is widely used in loud-speakers and voice coils.

The frequency response functions (FRFs) of a typical piezoelectric and electromagnetic PMAs mapping the voltage on the active element to the force generated by PMA is shown in Figure 2.2 and Figure 2.3, respectively. Clear from this frequency response function, PMAs have a rather limited effectiveness at lower frequencies, acceptable and somewhat frequency-independent effectiveness at high frequencies and are highly effective around their natural frequencies.

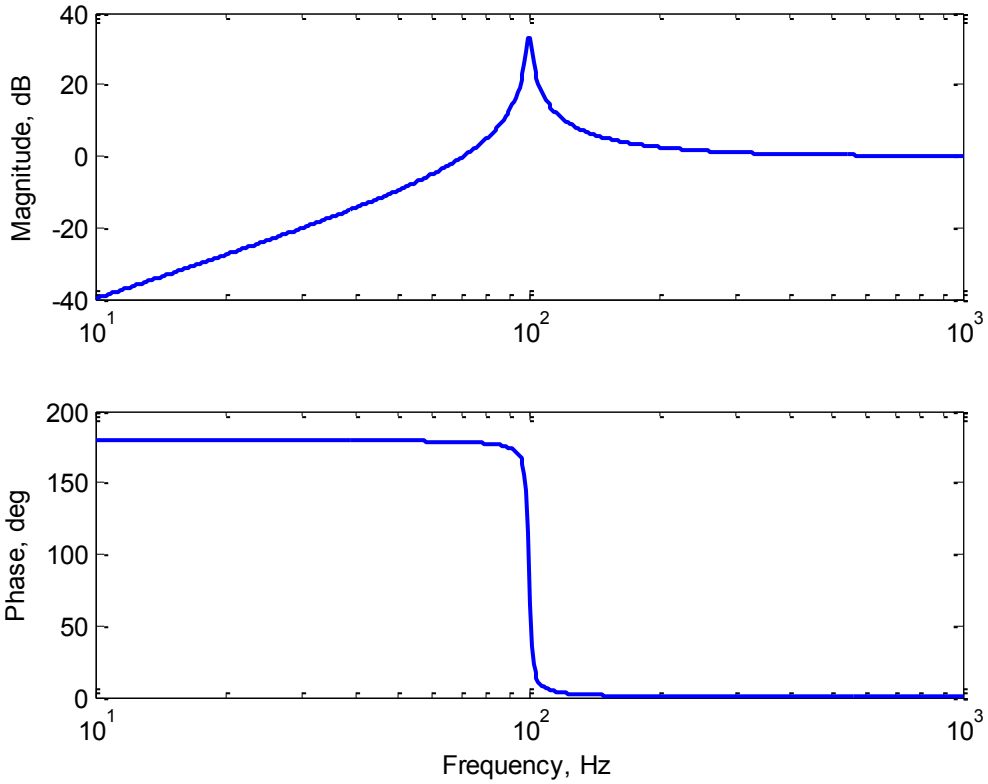

Figure 2.2: Typical FRF of a piezoelectric PMA

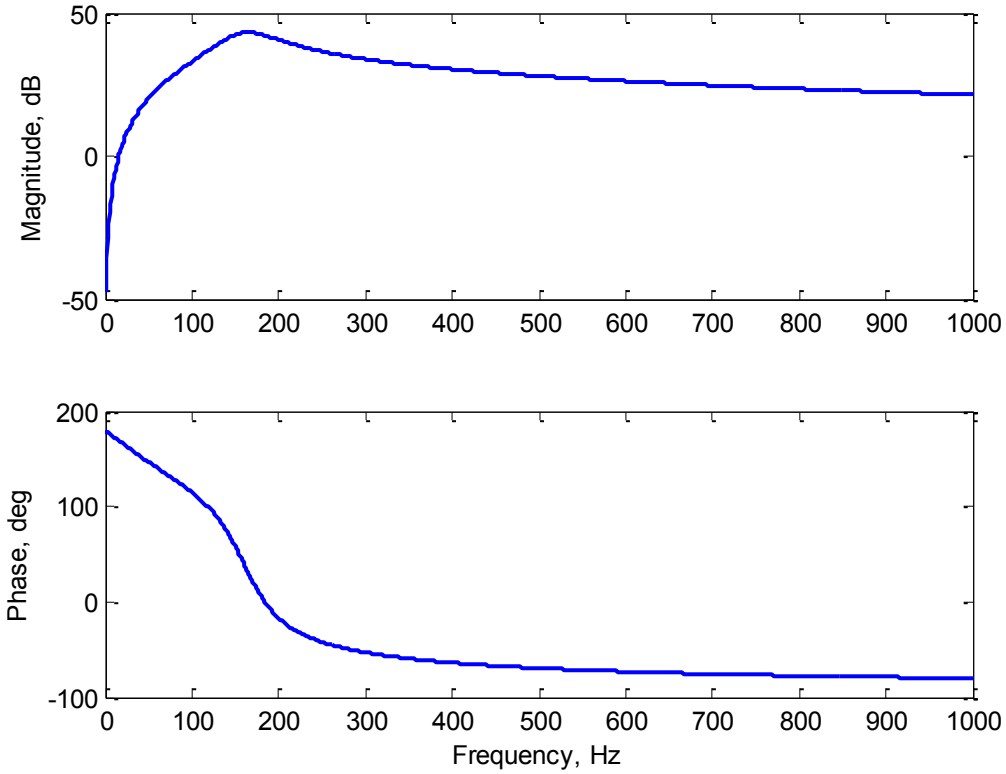

Figure 2.3: Typical FRF of an electromagnetic PMA

2.3 Experimental Evaluation

Frequency response functions (FRFs) of a PMA can be evaluated experimentally by installing the PMA on a rather massive structure (e.g. a large block of mass), driving it, and measuring the acceleration of the proof mass. The image of Figure 2.4(a) shows such an experimental setup. Figure 2.4(b) shows the measured FRF of the piezoelectric PMA used in this project with a 150 gram proof mass as the inertial element. Note that the natural frequency of the piezoelectric PMA is measured at around 340Hz. Similarly, the electromagnetic PMA with a proof mass of 417 gram is also evaluated in the same way as

shown in Figure 2.5. The natural frequency of the electromagnetic PMA is measured to be around 130Hz.

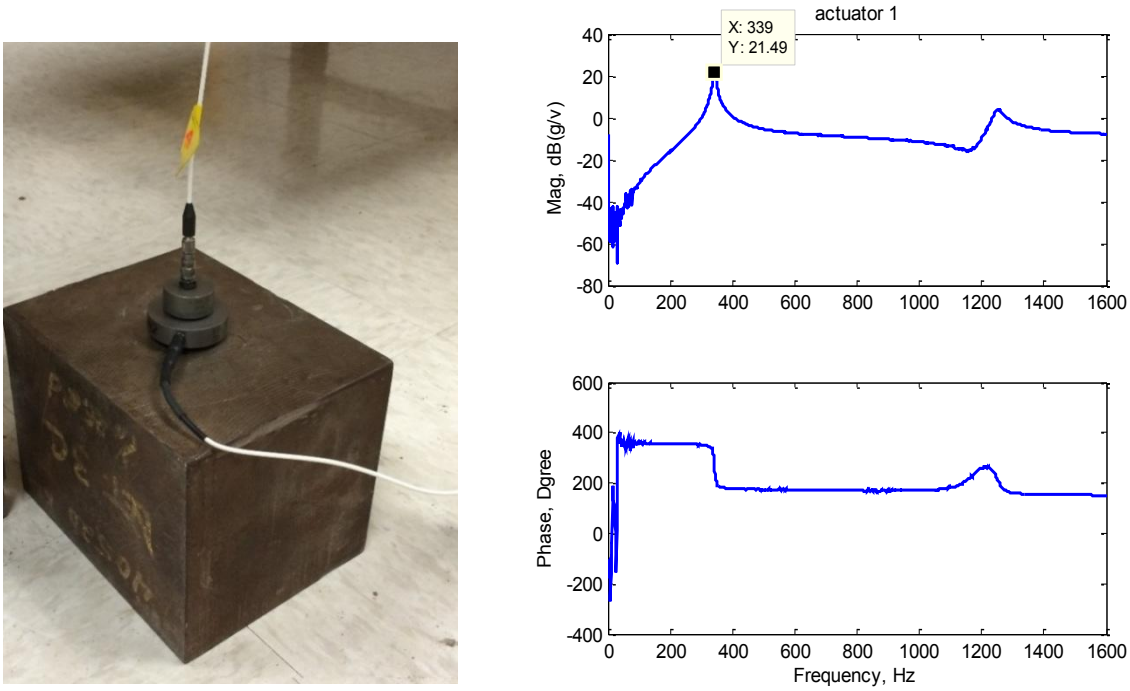

(a) (b)

Figure 2.4: The experimental setup (a) and measured FRF of the piezoelectric PMA (b)

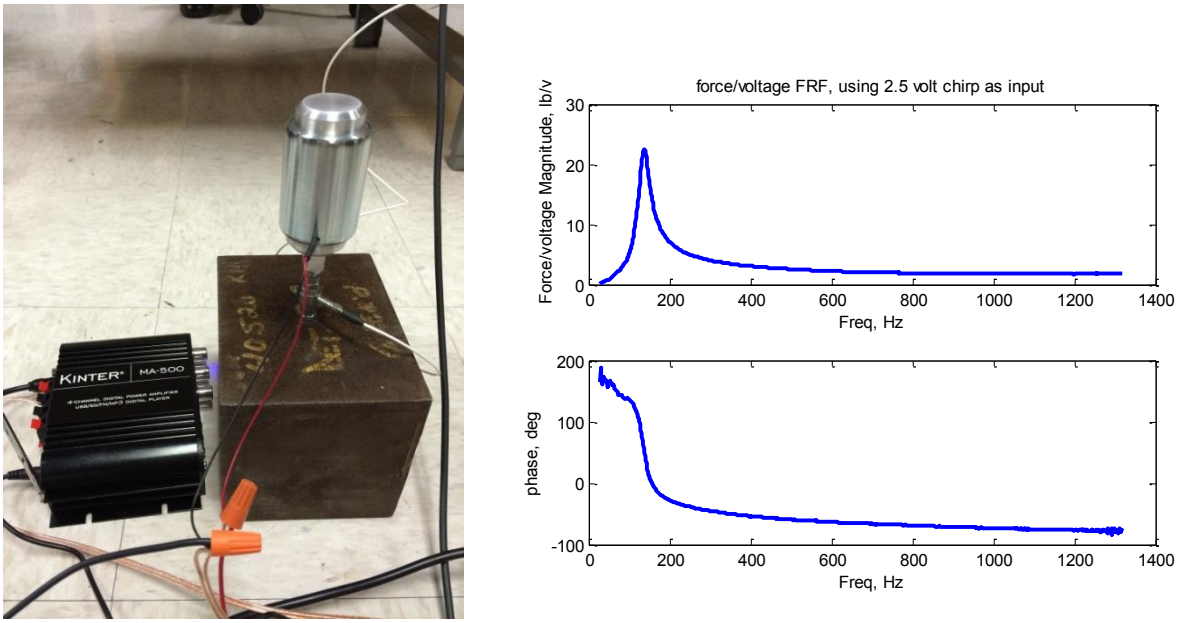

(a) (b)

Figure 2.5: The experimental setup (a) and measured FRF of the electromagnetic PMA (b)

It should be noted that, a TMD and a PMA have much in common. A TMD consists of a spring, a mass, and a damper. And a PMA is made up of a spring, a mass, a damper plus an actuation element. The schematic diagrams of the two systems are shown in Figure 2.6.

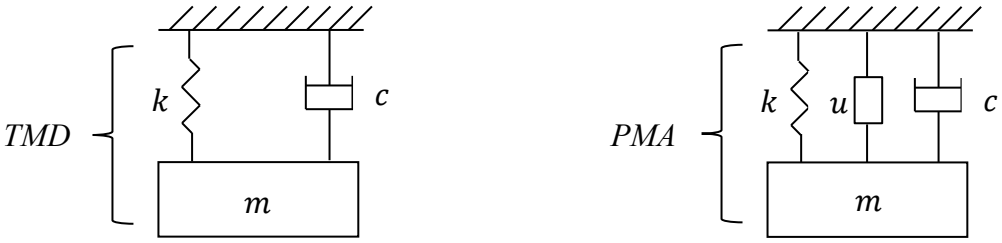

(a) (b)

Figure 2.6: Schematic diagram of a TMD (a) and a PMA (b)

CHAPTER III

LABORATORY EVALUATION

3.1 Introduction

The first of the control strategies discussed in chapter 1 was used in active vibration control of a beam, with the goal of damping one or multiple resonant modes as well as abating the forced vibration at the disturbing frequency. The feedback control adding damping to a target mode of vibration was fashioned after the dynamics of a TMD and the one used to abate the forced vibration was fashioned after the dynamics of a DA. These two control algorithms are dubbed TMD control and DA control in this write up. This control scheme is straightforward to implement and is highly effective but consumes more power than the second control scheme.

3.2 Experimental Setup

A 24.75 × 27/16 × 19/32 inch steel beam with free-free boundary conditions was used in the laboratory experiments. As shown in Figure 3.1 the nearly free-free boundary conditions are realized by suspending the beam.

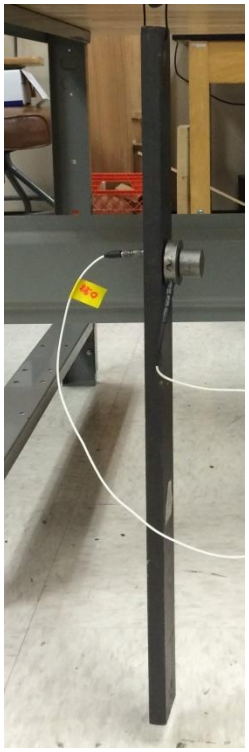

Figure 3.1: Experimental setup of the free-free beam

3.3 FE Model Analysis of the Beam

Finite element analysis (FEA) was first conducted to get the natural frequencies and mode shapes of the beam. As in any continuous parameter structure, the beam has infinite degrees of freedom modes. Considering the impracticality of modeling all the modes of the beam, only the first two modes with the corresponding frequencies of less than 1KHz, shown in Figure 3.2, were included in the model. The state space model of the beam was formulated using the model parameters.

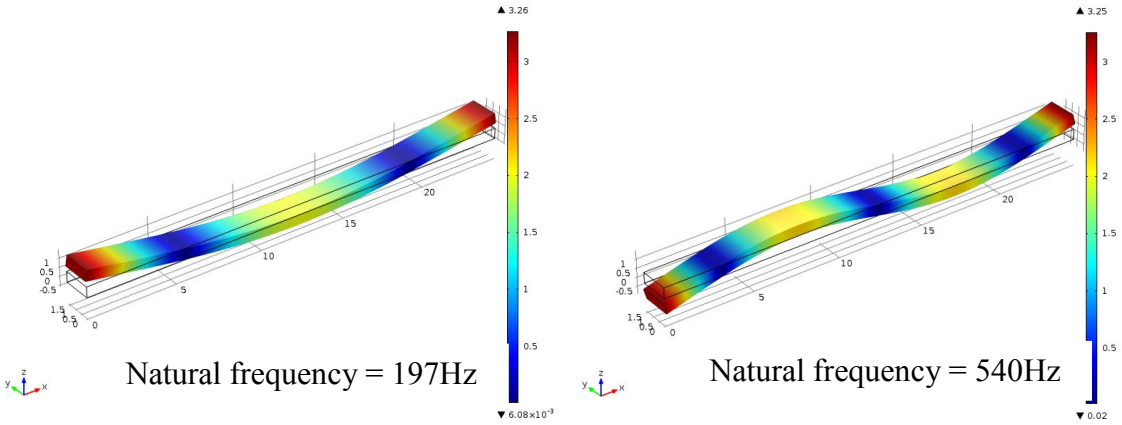

(a) (b)

Figure 3.2: The 1st (a) and 2nd (b) modes of the beam

The natural frequency of the piezoelectric PMA used in this experiment was between the frequencies of the 1st and 2nd mode of the beam. The 2nd mode was the targeted mode with its natural frequency close to the frequency where the test vehicle has the noise issue, i.e. ~ 500Hz. With the natural frequency of the 2nd mode well beyond the natural frequency of the PMA, the requirement for the first control strategy was satisfied. What is more, it is clear that one third length location of the beam where the PMA and the sensor (an accelerometer) were installed in a nearly co-located arrangement in Figure 3.1 has an anti-node shown in Figure 3.2(b). The goal of the experiment is to a) add damping to the 1st (not necessarily since does not have much effectiveness) and the 2nd mode, and b) absorb vibration of the beam at 750Hz.

3.4 Control Modeling

3.4.1 State Space Formulation of the Structure

In structural dynamics, displacements and velocities (in physical or modal domains) are the most commonly used states in state space models. The formulation presented by Equation (3.1) is the basis for state space modeling of flexible structures, in modal domain, having point force(s) as the input(s) and displacement(s) at discrete locations on the structure as the output(s).

$$\begin{aligned} \dot{z} &= \underbrace{\begin{bmatrix} 0 & I \\ -w_n^2 & -2\xi w_n \end{bmatrix}}_{A_1} z + \underbrace{\begin{bmatrix} 0 \\ Q \end{bmatrix}}_{B_1} u \\ y &= \underbrace{\begin{bmatrix} W & 0 \end{bmatrix}}_{C_1} z + \underbrace{\begin{bmatrix} D \end{bmatrix}}_{D_1} u \end{aligned} \tag{3.1}$$

where

State vector: $z(t) = [q(t) \quad \dot{q}(t)]$

Number of modes: Nm

Number of inputs: Nu

Number of outputs: Ny

Modal displacement: $q(t) = [q_1(t) \quad q_2(t) \quad ... \quad q_{Nm}(t)]'$

Modal velocity: $\dot{q}(t) = [\dot{q}_1(t) \quad \dot{q}_2(t) \quad ... \quad \dot{q}_{Nm}(t)]'$

Input: $u = \begin{bmatrix} u_1 & u_2 & ... & u_{Nu} \end{bmatrix}'$

Natural frequency: $W_n = diag(\begin{bmatrix} W_{n1} & W_{n2} & ... & W_{nNm} \end{bmatrix})$

Modal damping ratio: $\zeta = diag(\begin{bmatrix} \zeta_1 & \zeta_2 & ... & \zeta_{Nm} \end{bmatrix})$

Spatial coordinate: r

Mode_i: $\Psi_i(r)$

Modal input matrix: $Q(r) = [\Psi_1(r) \quad \Psi_2(r) \quad ... \quad \Psi_{Nu}(r)]'$ (evaluated at the input locations)

Modal output matrix: $W(r) = \left[\Psi_1 \quad \Psi_2 \quad ... \quad \Psi_{Ny}(r)\right]$ (evaluated at the output locations)

Clear from Equation (3.1), the A_1, B_1, C_1, D_1 matrices describing the structure's state-space model in modal domain, are functions of the modal parameters of the system (natural frequencies, modal damping ratios, and mode shapes).

3.4.2 State Space Formulation of the PMA

The schematic diagram of Figure 3.3, depicting a PMA appended to a one degree of freedom structure, is used to develop the model of a structure actively controlled by a PMA. In Figure 3.3, m_1, k_1, c_1 are the parameters (mass, stiffness and damping coefficient) of the structure, m_2, k_2, c_2 are the parameters of the PMA, and x_1, x_2 are the displacement of the structure and PMA, respectively.

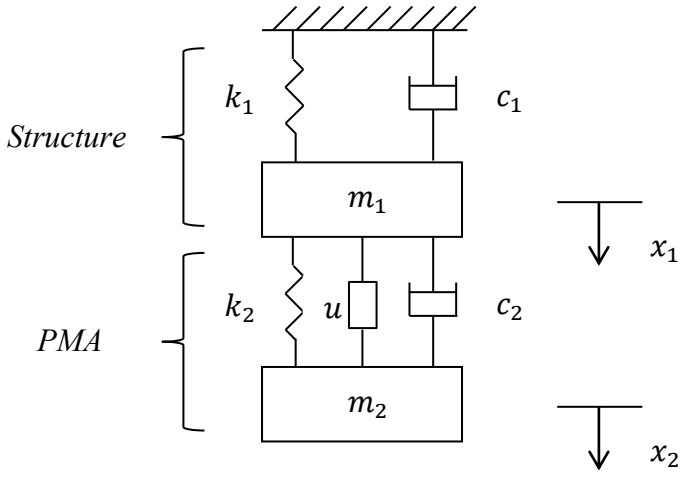

Figure 3.3: Schematic diagram of PMA appended to a structure

First, we viewed the PMA as a tuned mass damper (TMD) and developed its (the TMD"s) model. Note that the difference between a PMA and a TMD is the presence of an active element (u) in the PMA. Equation (3.2) shows the transfer function of the TMD with the displacement of the structure, where the TMD is appended to, as the input and the force in the TMD suspension as the output.

$$\frac{TMD_{force}}{structure_{disp}} = \frac{m_2 s^2 (c_2 s + k_2)}{m_2 s^2 + c_2 s + k_2} \tag{3.2}$$

To be able to extend the model of the TMD shown by Equation (3.2) to that of a PMA and subsequently use that model in the development of controlled plant (structure plus PMA), the transfer function of Equation (3.2) needs to be reformulated in state space format. To do this, first the non-rational transfer function of Equation (3.2) needs to be rearranged to a rational one. This was done in the two steps of a) rewriting Equation (3.2) as Equation (3.3)

$$TMD_{force} = \frac{m_2 s^2}{m_2 s^2 + c_2 s + k_2} (c_2 s + k_2) * structure_{disp} \tag{3.3}$$

and b) viewing the term $(c_2 s + k_2) * structure_{disp}$ as the summation of damping force and stiffness force of the structure, i.e. $c_2 v_1 + k_2 x_1$ where x_1 and v_1 are the displacement and velocity[2] of the structure where the TMD is installed. This in turn changes Equation (3.3) to Equation (3.4).

$$TMD_{force} = m_2 \frac{s^2}{m_2 s^2 + c_2 s + k_2} (c_2 v_1 + k_2 x_1) \tag{3.4}$$

Equation (3.4) is presented in block diagram format of Figure 3.4.

[2] Note that s in Laplace domain is equivalent to differentiation in time domain.

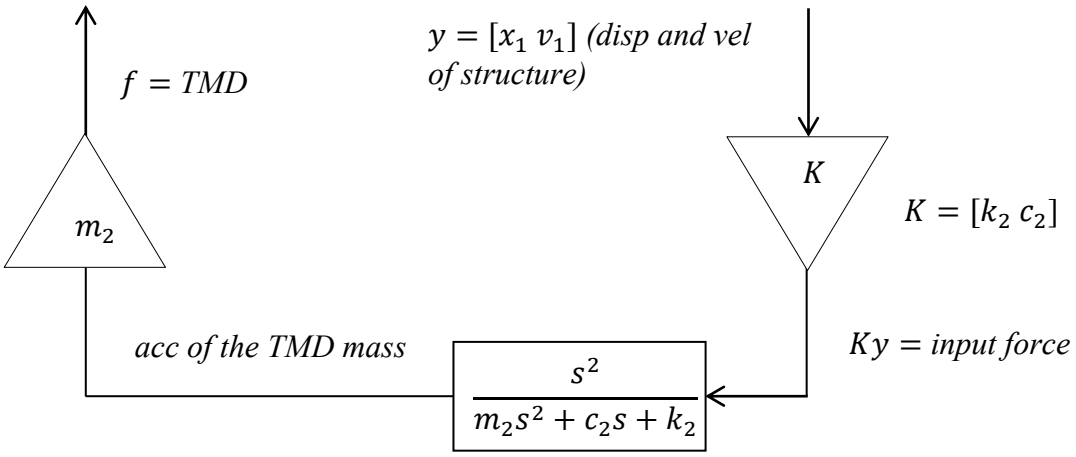

Figure 3.4: A block diagram model of TMD

To formulate the model of the TMD shown in Figure 3.4 in state space format, first the equation of motion of the TMD mass i.e. Equation (3.5) is looked at

$$m_2\ddot{x}_2 + c_2\dot{x}_2 + k_2x_2 = c_2\dot{x}_1 + k_2x_1 \tag{3.5}$$

where x_1 and x_2 are the displacements of structure and TMD, respectively.

Setting $K = \begin{bmatrix} k_2 & c_2 \end{bmatrix}$, $y = \begin{bmatrix} x_1 \\ \dot{x}_1 \end{bmatrix}$ and dividing both sides by m_2, Equation (3.5) is written as Equation (3.6).

$$\ddot{x}_2 + \frac{c_2}{m_2}\dot{x}_2 + \frac{k_2}{m_2}x_2 = \frac{1}{m_2}Ky \tag{3.6}$$

Defining the displacement x_2 and velocity v_2 of the TMD mass as the states, Equation (3.6) is reformulated in the state and output Equations of (3.7) and (3.8).

$$\begin{bmatrix} \dot{x}_2 \\ \dot{v}_2 \end{bmatrix} = \begin{bmatrix} 0 & 1 \\ -\frac{k_2}{m_2} & -\frac{c_2}{m_2} \end{bmatrix} \begin{bmatrix} x_2 \\ v_2 \end{bmatrix} + \begin{bmatrix} 0 \\ \frac{1}{m_2} \end{bmatrix} Ky \tag{3.7}$$

$$a_2 = \begin{bmatrix} -\frac{k_2}{m_2} & -\frac{c_2}{m_2} \end{bmatrix} \begin{bmatrix} x_2 \\ v_2 \end{bmatrix} + \frac{1}{m_2}Ky \tag{3.8}$$

where $a_2 = \dot{v}_2$, i.e., the acceleration of the TMD mass is the output and Ky is the input. Multiplying the output Equation (3.8) by the mass of TMD, m_2 , changes the output of the state space model to TMD force, shown in Equation (3.9) .

$$\begin{bmatrix} \dot{x}_2 \\ \dot{v}_2 \end{bmatrix} = \underbrace{\begin{bmatrix} 0 & 1 \\ -\frac{k_2}{m_2} & -\frac{c_2}{m_2} \end{bmatrix}}_{A_2} \begin{bmatrix} x_2 \\ v_2 \end{bmatrix} + \underbrace{\begin{bmatrix} 0 \\ \frac{1}{m_2} \end{bmatrix}}_{B_2} Ky \tag{3.9}$$

$$f = \underbrace{\begin{bmatrix} -k_2 & -c_2 \end{bmatrix}}_{C_2} \begin{bmatrix} x_2 \\ v_2 \end{bmatrix} + \underbrace{1}_{D_2} * \mathrm{Ky}$$

As will be discussed in the next section, the introduction of the actuation extends the state space model of TMD to that of PMA.

3.4.3 Structure Plus PMA Model

Interfacing the structure model to that of the TMD shown in Figure 3.4 results in the block diagram model of the structure plus TMD shown in Figure 3.5. The -1 gain in the block diagram signifies the negative feedback nature of the loop.

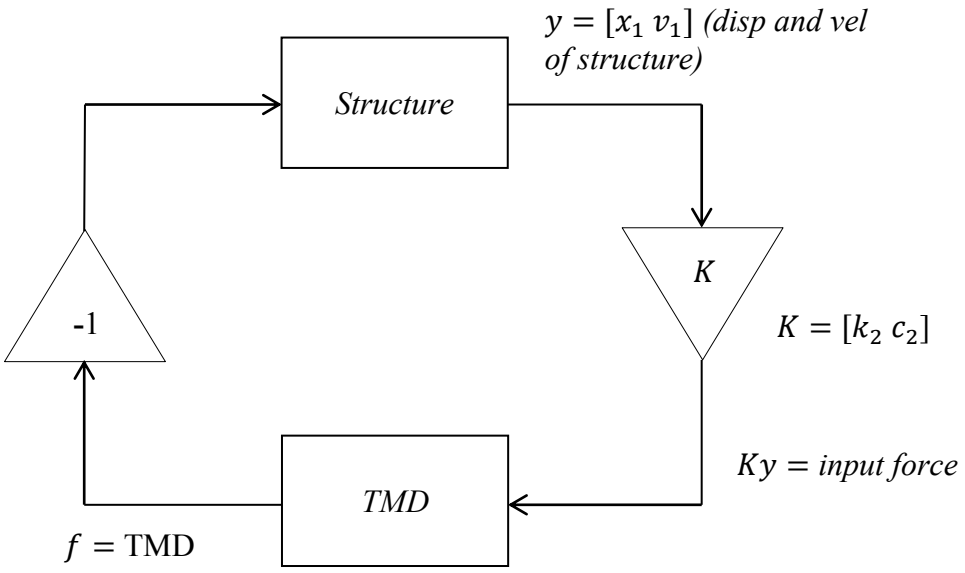

Figure 3.5: The block diagram model of TMD appended to a structure

The addition of the control input *u* to the TMD block of Figure 3.5 changes the tuned mass damper model to the model of a PMA. This, in turn, modifies the block diagram of Figure 3.5 to that of Figure 3.6[3]. As shown in the state space model of the TMD presented by Equation (3.9), the TMD force is $m_2 * acc$. Considering that the inertial force of the TMD mass is also the suspension (spring + viscous damper + actuator) force of the TMD, it is sufficient to input the control force *u* only on the TMD block and not on the structure block of Figure 3.6. In addition, when the PMA is used to both perturb and control the structure, the synthetic disturbance input, similar to the control force *u*, acts on the TMD only.

[3] Note that PMA has the same state space formulation as that of TMD.

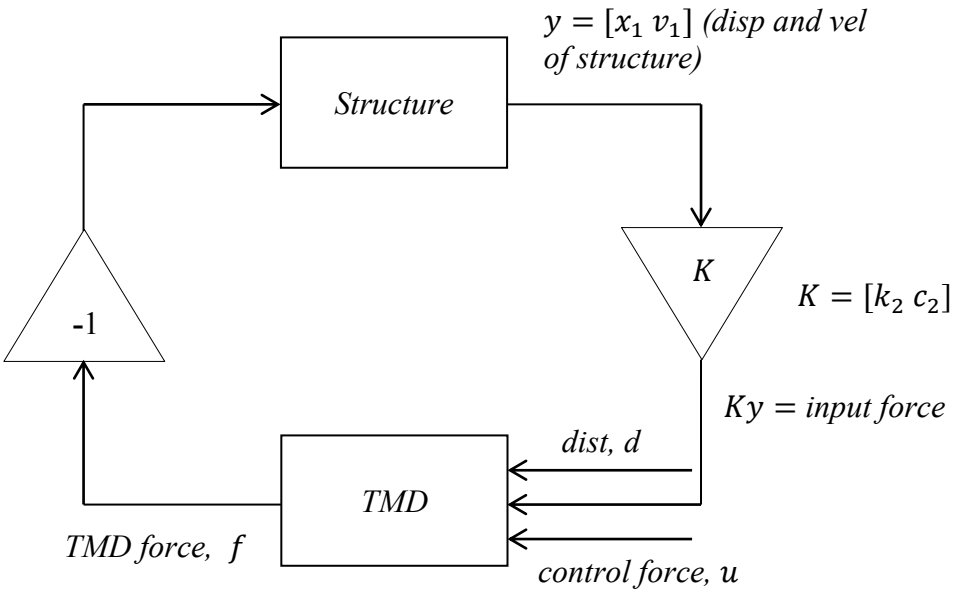

Figure 3.6: The block diagram of PMA appended to a structure

3.4.4 The State Space Model of Structure Plus PMA

The state space formulation of the structure and the PMA is shown by Equations (3.10) through (3.13) where *d*, *f* and *u* represent the disturbance, PMA force, and control force, respectively. Note that D_1 is zero.

Structure:

$$\dot{x}_1 = A_1 x_1 + B_1 f \tag{3.10}$$

$$y = C_1 x_1 + D_1 f = C_1 x_1 \qquad D_1 = 0 \tag{3.11}$$

PMA:

$$\dot{x}_2 = A_2 x_2 + B_{21} d + B_{22} K y + B_{23} u \tag{3.12}$$

$$f = C_2 x_2 + D_{21} d + D_{22} K y + D_{23} u \tag{3.13}$$

In order to combine the structure and the PMA into one state space formulation, the procedure outlined in the following steps of 1 thru 4 and Equations (3.14) through (3.18) are performed.

1. Substitute for f in Equation (3.10) from Equation (3.13)

$$\dot{x}_1 = A_1 x_1 + B_1 (C_2 x_2 + D_{21} d + D_{22} K y + D_{23} u) \tag{3.14}$$

2. Substitute for y in Equation (3.14) from Equation (3.11)

$$\dot{x}_1 = A_1 x_1 + B_1 C_2 x_2 + B_1 D_{21} d + B_1 D_{22} K C_1 x_1 + B_1 D_{23} u \tag{3.15}$$

$$\dot{x}_1 = (A_1 + B_1 D_{22} K C_1) x_1 + B_1 C_2 x_2 + B_1 D_{21} d + B_1 D_{23} u \tag{3.16}$$

3. Substitute for y in Equation (3.12) from Equation (3.11)

$$\dot{x}_2 = B_{22} K C_1 x_1 + A_2 x_2 + B_{21} d + B_{23} u \tag{3.17}$$

4. Combine Equation (3.16), (3.17) and (3.11) we can get the state space formulation of a PMA appended to a structure.

$$\dot{x} = \underbrace{\begin{bmatrix} A_1 + B_1 D_{22} K C_1 & B_1 C_2 \\ B_{22} K C_1 & A_2 \end{bmatrix}}_{A} x + \underbrace{\begin{bmatrix} B_1 D_{21} \\ B_{21} \end{bmatrix}}_{B_{dist}} d + \underbrace{\begin{bmatrix} B_1 D_{23} \\ B_{23} \end{bmatrix}}_{B_{control}} u \tag{3.18}$$

$$y = \underset{C}{C_1}\, x_1$$

In Equation (3.18), $\dot{x}$ is the vector of two velocities $\begin{bmatrix} \dot{x}_1 \\ \dot{x}_2 \end{bmatrix}$. The B matrix contains the two parts of B_{dist} in the first column and $B_{control}$ in the second column. The D matrix is zero in this state space formulation.

3.4.5 Numerical Modeling and Verification

The state space model of the structure with disturbance force as the input and acceleration as the output was constructed using the modal parameters of the structure evaluated by finite element modal analysis. The FRF of the state space model of the structure was compared well with the experimentally measured[4] FRF, pointing to the fidelity of the state space model using the frequency response functions as the metric. Figure 3.7 shows the magnitude of the two FRFs.

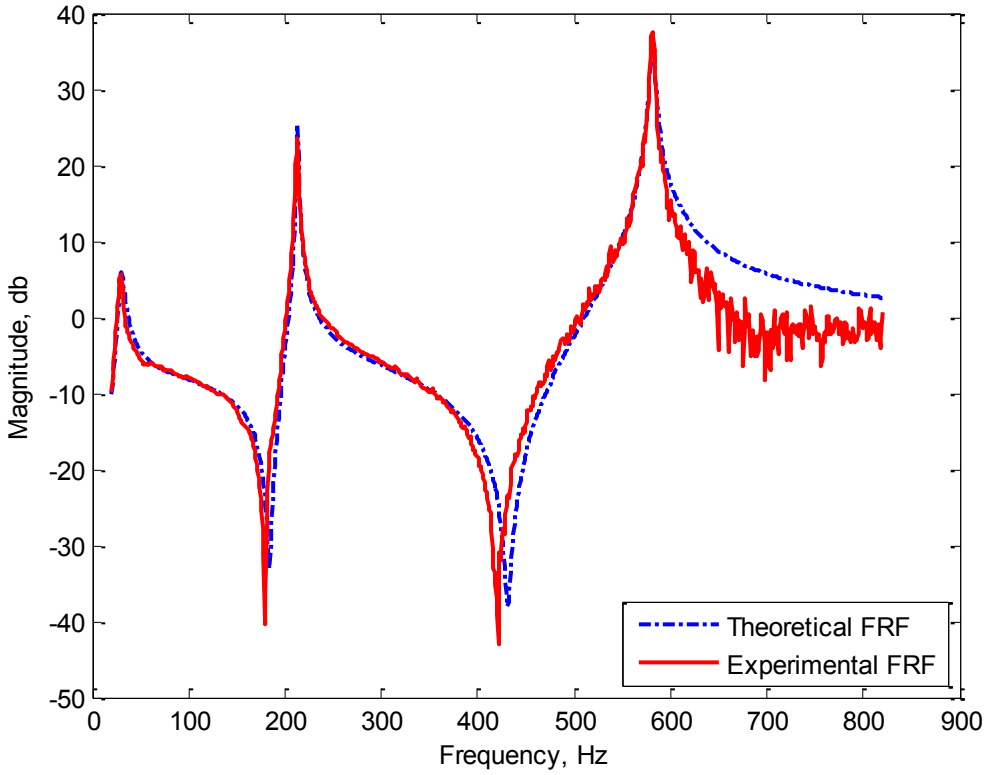

Figure 3.7: Numerically and experimentally evaluated FRFs of the structure

[4] The experimental FRF was evaluated by perturbing the structure using an instrumental hammer and measuring the acceleration by a nearly co-located accelerometer.

Augmenting the verified model of the structure with the model of the PMA, resulted in the model of the plant (structure plus PMA). The numerical model of the plant also compared well with the experimentally measured one. Figure 3.8 compares the two numerically and experimentally evaluated FRFs. The FRFs were generated using the PMA force as the perturbation (input) and the acceleration measured by a nearly co-located (with the PMA) accelerometer as the output.

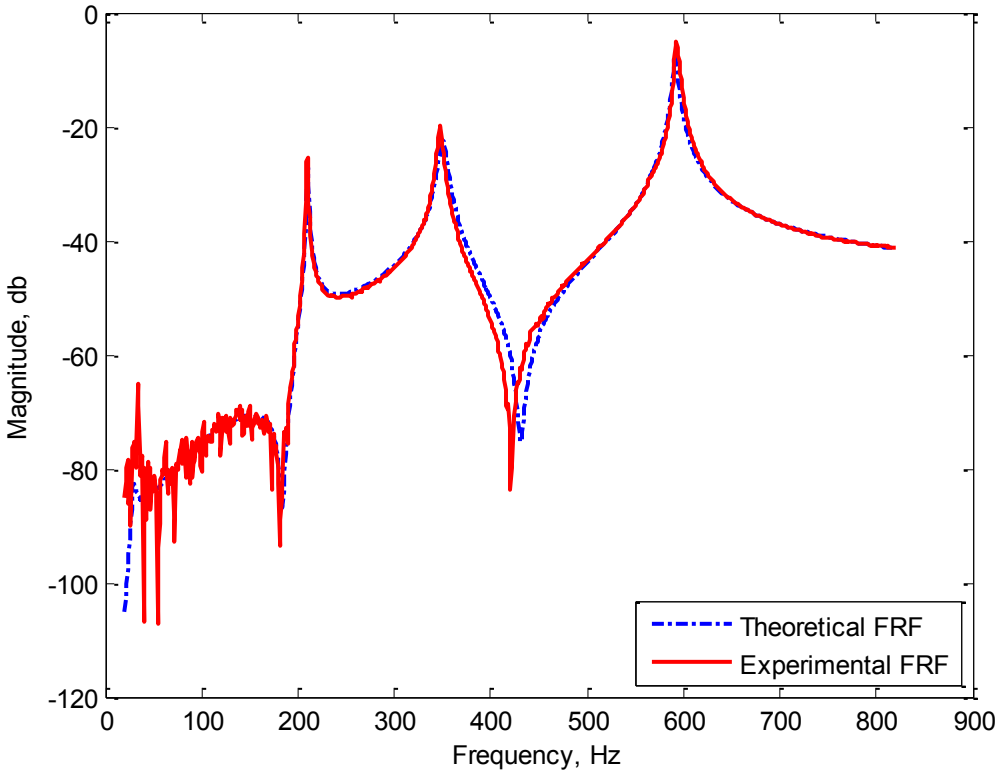

Figure 3.8: Numerically and experimentally evaluated FRFs of the plant (structure plus PMA)

3.5 Controller Design

With the state space model of the plant formulated and experimentally verified, the next step was designing the controller. With the goal of adding tuned damping and/or tuned vibration absorption to the structure, TMD and DA controllers fashioned after the

dynamics of a passive TMD and DA[5] were designed and implemented both numerically and experimentally. The common transfer function of these controllers, is shown in Equation (A-4) of Appendix A. What distinguishes TMD controller from DA controller is the extent of damping in the transfer function Equation (A-4). These controllers are rather straightforward to design and implement, using a PMA as the control actuator, as long as the natural frequency of the PMA itself is placed well below the frequency of intent targeted for tuned damping and/or tuned vibration absorption.

3.6 TMD + Basic DA Control

Evident from Figure 3.8, the system (structure plus PMA) has three modes in the 100-900Hz frequency range. The 1st mode (around 200Hz) and the 3rd mode (around 600Hz) are the modes of the beam. The 2nd mode (around 340Hz, matching the natural frequency of the PMA shown in Figure 2.4(b)) is the mode of the PMA. A TMD controller was used to damp the 1st mode (with minimal effectiveness) and 3rd mode of the system. Moreover, with an external excitation force (causing forced vibration) at the frequency of 750Hz, a DA controller tuned to that frequency was used to absorb corresponding forced vibration of the structure. The block diagram of the combined TMD and basic DA controlled system is shown in Figure 3.9.

[5] See appendix A for the formulation of the TMD and DA dynamics

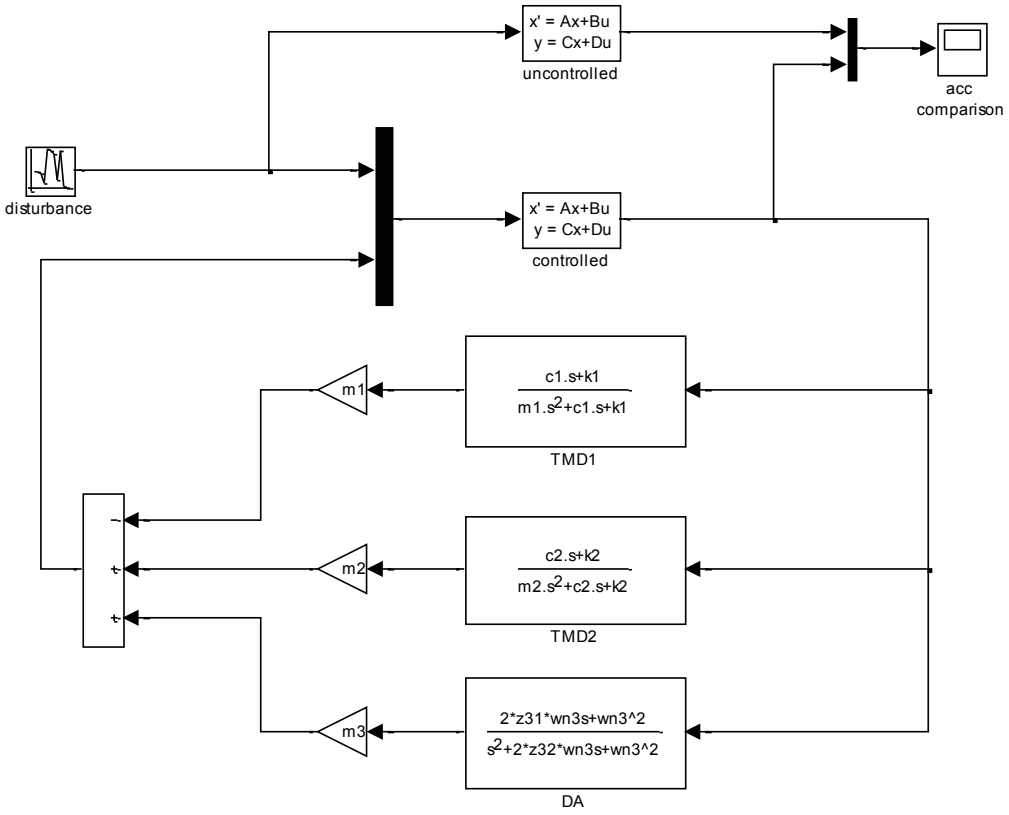

Figure 3.9: Block diagram of the TMD + basic DA controlled system

As shown in the block diagram of Figure 3.9, three controllers were used in this simulation for the 1st mode, 3rd mode (TMD 1 and TMD 2) and external excitation (DA) respectively. The uncontrolled structure was also included in the model of Figure 3.9, for comparison purposes, to show the effectiveness of the controller against. The FRFs mapping the perturbation input to the acceleration output of the structure without and with control were evaluated and are presented in Figure 3.10. Note that acceleration was evaluated at the same location as the actuator position.

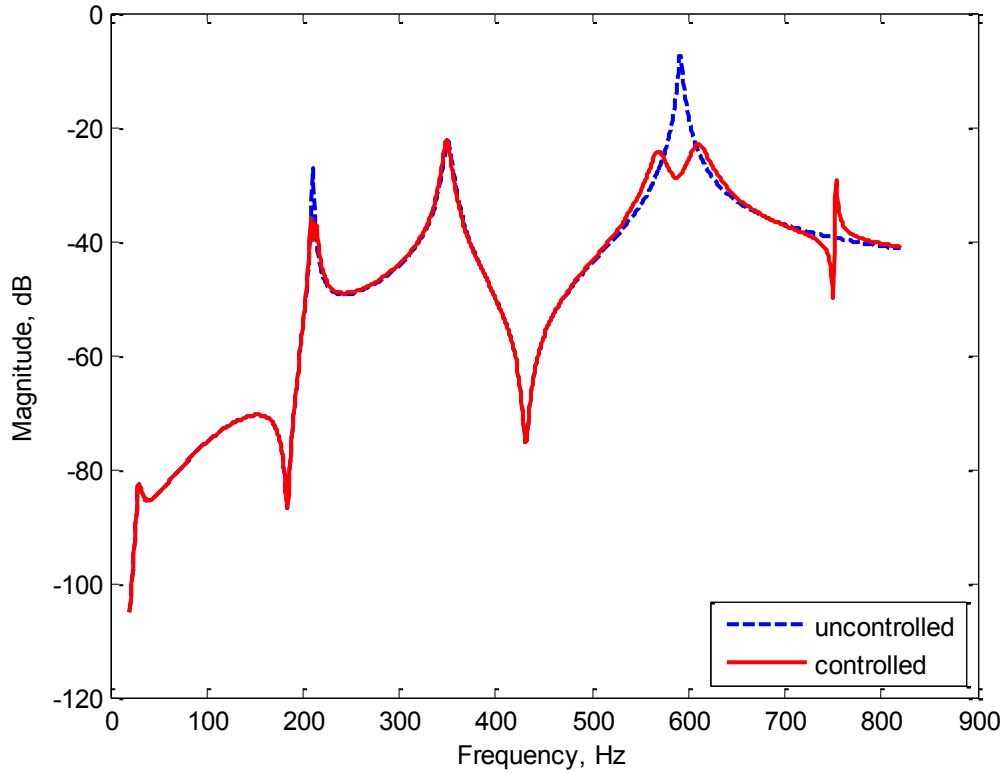

Figure 3.10: Numerically evaluated FRFs mapping the perturbation input to the acceleration output without (blue trace) and with (red trace) basic TMD + DA controller

Clear from Figure 3.10, the first active vibration control strategy introduces a desirable amount of damping to the 1st mode and 3rd mode of the structure. It also absorbs the forced vibration at 750Hz. Following this numerical exercise, an experiment was conducted, by shaking the free-free beam with a PMA and adding control by the same PMA[6]. The experimental setup is shown in Figure 3.1.

A digital signal analyzer (DSA) generated a disturbance signal to drive the PMA perturbing the beam. Meanwhile, the control signal from the control computer was added to the disturbance signal to reduce vibration of the beam. The control signal was turned

[6] Note that the PMA is a linear system which can deal with the perturbation and control at the same time.

off and on to set the beam to be in the stage of uncontrolled and controlled. The block diagram of the controller residing in the control computer is shown in Figure 3.11.

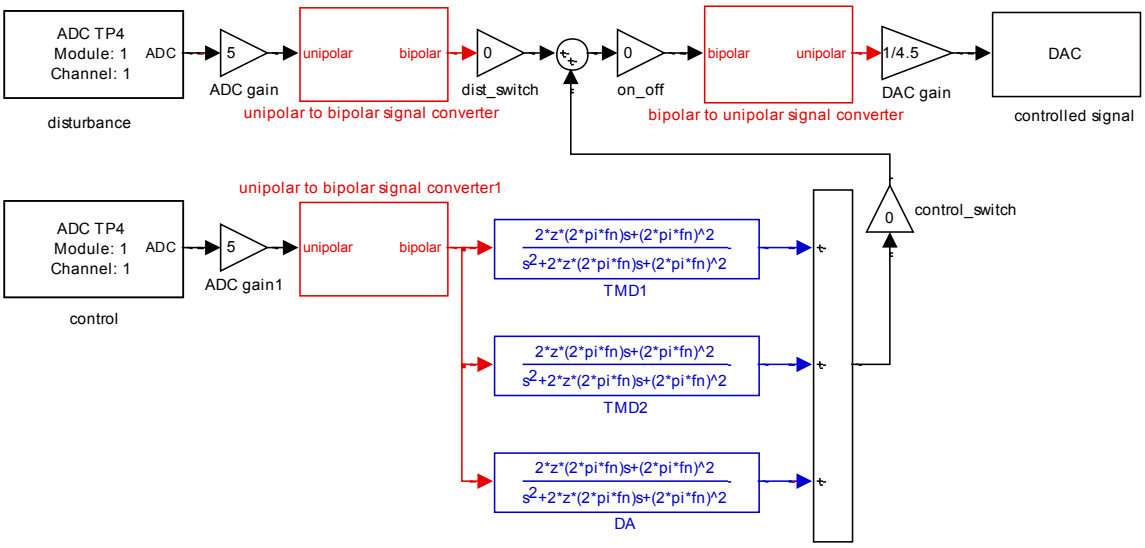

Figure 3.11: TMD_DA control interface

In Figure 3.11, the blocks represent the parallel cascade of 3 individual controllers that make up the overall control. fn and z in the blocks represent the natural (tuning) frequency and damping ratio of each controller. Additional analog hardware for converting unipolar to bipolar signals and vice-versa[7] were also used in this experiment.

The FRFs mapping the disturbance to the measured acceleration of the uncontrolled and controlled structure (the beam) are shown in Figure 3.12. Band limited, random disturbance with the frequency content of 100-900Hz was used to perturb the beam. Almost 20dB effectiveness (10 times reduction) is obtained in the 3rd mode. Moreover, at the frequency to which the DA controller is tuned, a substantial absorption

[7] The A/D and D/A convertors of the control computer are unipolar devices.

of vibration is realized. Note that the experimentally measured FRFs of Figure 3.12 are very similar to the numerically evaluated ones of Figure 3.10.

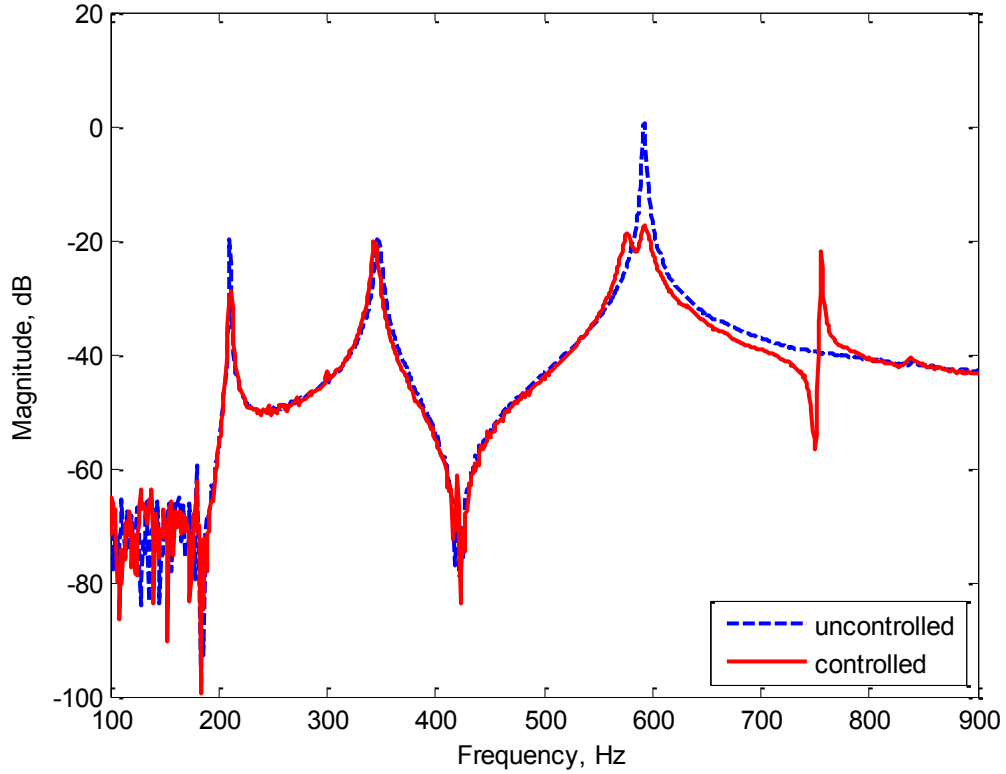

Figure 3.12: Experimentally measured FRF mapping the perturbation input to the acceleration without (blue trace) and with (red trace) basic TMD_DA control

In another experiment, two single frequency disturbances at 592Hz (the frequency of the 2nd mode targeted for active damping) and 750Hz (the forced vibration frequency) were used to perturb the system. The abatement of the audible structure-borne noise caused by the vibration of the beam was clearly distinguishable, when the controller was turned on.

3.7 Modified DA Controller

The DA controller transfer function is fashioned after the second order dynamics of mechanical dynamic absorber made up of highly underdamped spring-mass-damper system. Mechanical dynamic absorbers are normally used to absorb forced vibration of a structure at a forcing frequency which is not in the vicinity of a resonant frequency[8]. The transfer function of a structure over the frequencies away from resonant frequencies can be approximated as $\frac{acc}{force} = \frac{1}{M}$, where M is the mass of the structure. The block diagram model of such structure, treated with a mechanical dynamic absorber is shown in Figure 3.13, with the overall transfer function of

$$\frac{acc}{dist} = \frac{1}{M} \frac{s^2 + 2\xi w_n s + w_n^2}{s^2 + (1+\frac{m}{M})2\xi w_n s + (1+\frac{m}{M})w_n^2} \tag{3.19}$$

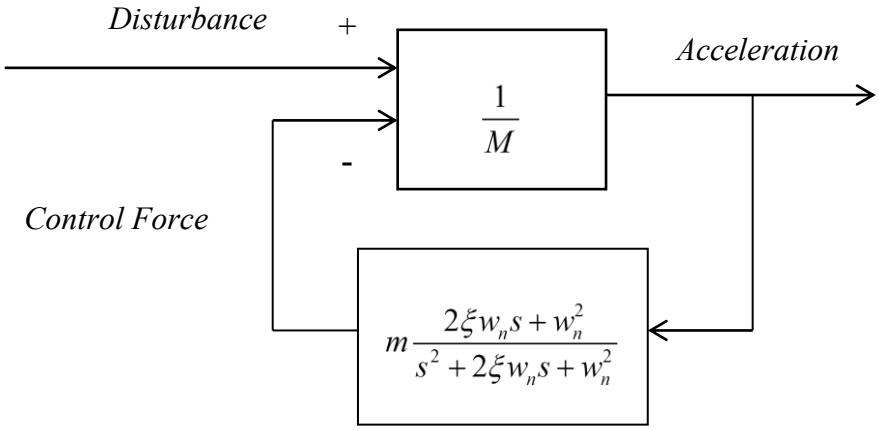

Figure 3.13: Schematic block diagram of a structure plus a DA

[8] When the forcing frequency is in the vicinity of a resonant frequency, tuned mass dampers are the more appropriate vibration control solution.

The very small damping ratio of the mechanical dynamic absorber ξ, results in a pair of complex conjugate zeros (the roots of the numerator of Equation (3.19)) responsible for placing the desirable notch, at the forcing frequency on the FRF of the controlled structure. Considering that $\frac{m}{M}$ is very small, the coefficient $1+\frac{m}{M}$ in the denominator of Equation (3.19) is almost equal to 1. With this approximation, the very small damping ratio of the dynamic absorber ξ also results in a pair of complex conjugate poles (the roots of the denominator of Equation (3.19)). This pair of highly underdamped poles creates an undesirable sharp peak next to the desirable notch. This creation of the peak, caused by the highly underdamped poles of Equation (3.19) could have been addressed had the damping ratio in the numerator of the dynamic absorber transfer function been made many times larger than the damping ratio in its denominator. Although not possible in a mechanical dynamic absorber, but this can be done in a DA controller. Modifying the transfer function of the DA controller from that of Equation (A-4) in Appendix A to

$$\frac{F}{acc} = m\frac{2(\alpha\xi)w_n s + w_n^2}{s^2 + 2\xi w_n s + w_n^2} \tag{3.20}$$

with $\alpha > 1$ (e.g. $\alpha = 10$), changes the transfer function of the structure actively treated by a DA controller to

$$\frac{acc}{dist} = \frac{1}{M}\frac{s^2 + 2\xi w_n s + w_n^2}{s^2 + (1+\frac{m}{M})2(\alpha\xi)w_n s + (1+\frac{m}{M})w_n^2} \tag{3.21}$$

Clear from Equation (3.21), the underdamped zeros creating the desirable notch in the FRF absorbing the forced vibration are unchanged, but the poles are now many times more damped resulting in a very shallow peak in the FRF of the DA controlled structure.

Figure 3.14 shows the FRFs of the structure without and with the DA controller of Equation (21). Comparison of the controlled system FRF in Figure 3.14 with that of Figure 3.12 shows the impact of modifying the DA controller dynamics from Equation (A-4) to Equation (20).

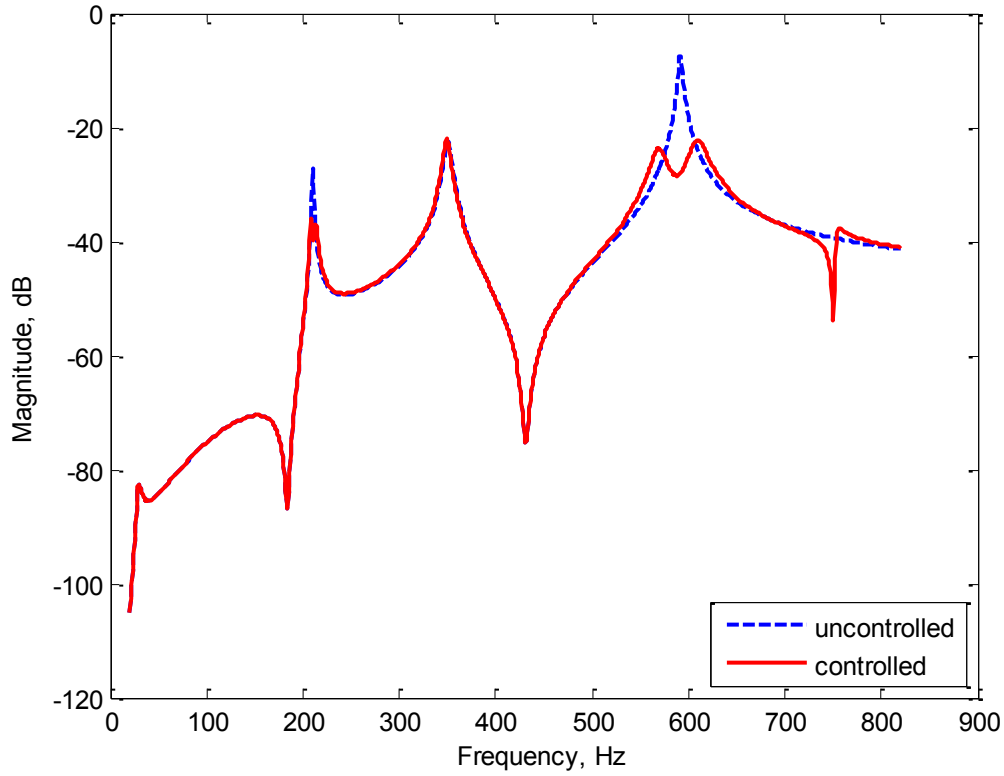

Figure 3.14: Theoretically measured FRF mapping the perturbation input to the acceleration without (blue trace) and with (red trace) improved DA controller

The peak around the tuning frequency of the DA controller has been almost wiped out without damaging the notch close to it. The modified DA controller was experimentally implemented on the beam and similar result to that of Figure 3.14, as shown in Figure 3.15, was achieved.

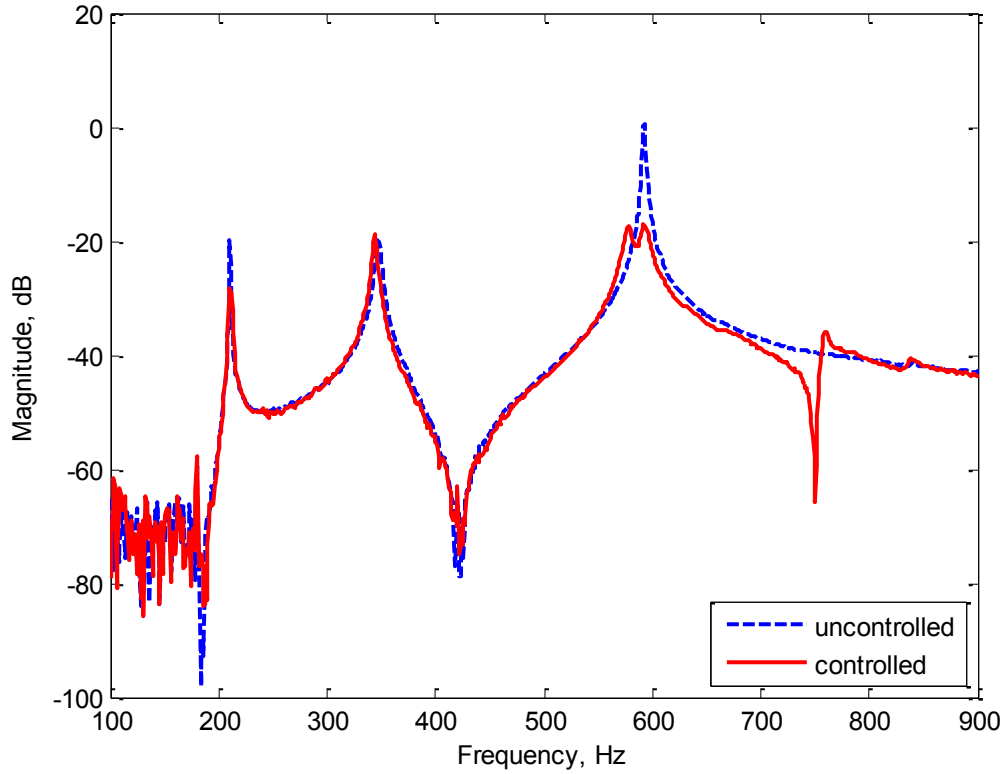

Figure 3.15: Experimentally measured FRF mapping the perturbation input to the acceleration without (blue trace) and with (red trace) improved DA controller

3.8 Active Damping

As the active element in vibration control application, PMA introduces its own resonance into the dynamics of the structure equipped with PMA. In the FRF of the PMA actuated beam shown in Figure 3.15, the 2nd mode at around the 340Hz is due to the dynamics[9] of the PMA itself. In other words, the beam tested in the previous experiments would not have had this mode without the PMA. If the disturbance to the structure happens to be at the frequency of the 2nd mode, the vibration created by the disturbance will be severe. The TMD controller targeting this mode does not work since the condition

[9] If the natural frequency of the PMA is not in the frequency range of interest, the presence of the PMA related resonance is immaterial.

for the control strategy 1 is not satisfied. There are two ways to solve this problem. Firstly, incorporate passive damping into the PMA itself. Secondly, add active damping via velocity feedback.

For a one degree of freedom (DOF) system, the damping in the system is proportional to the velocity of structure itself, i.e., the relative velocity between the structure and the ground, as it is shown in Figure 3.16. In the case discussed the relative velocity between the PMA and the beam is needed for incorporating active damping in the TMD_DA and active damping control.

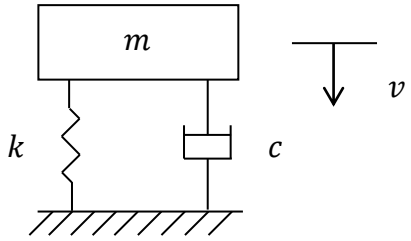

Figure 3.16: The schematic diagram of a one DOF structure

Adding damping to the PMA mode actively along with active tuned mass damping of the two of the structure"s modes were numerically explored and experimentally verified. Figure 3.17 shows the block diagram of the numerical model.

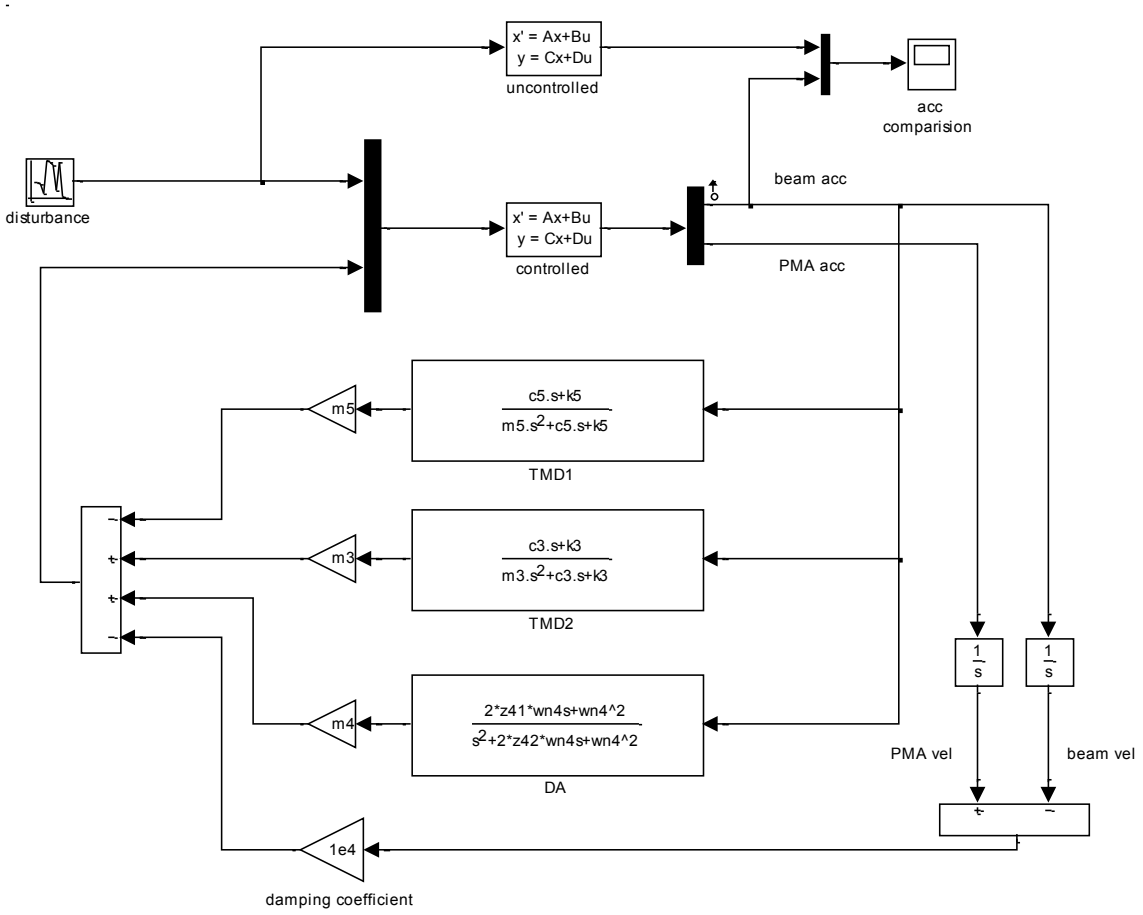

Figure 3.17: Simulation block diagram of the TMD_DA and active damping control

In Figure 3.17, the controllers work in a parallel. The numerical FRFs of the beam uncontrolled (dashed line) and controlled (solid line) by two TMD controllers tuned to 200 and 600Hz, a DA controller tuned to 750Hz and a relative velocity feedback controller to dampen the PMA‟s 340Hz mode are shown in Figure 3.18.

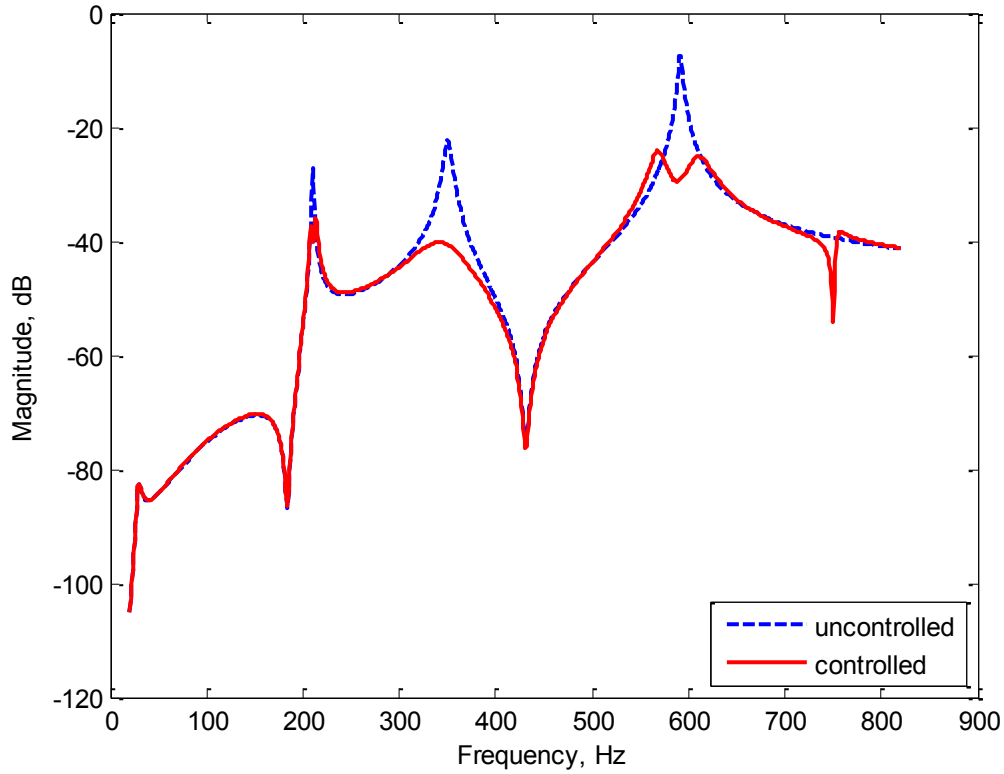

Figure 3.18: Numerically measured FRF mapping the perturbation input to the acceleration without (dashed line trace) and with (solid line trace) TMD_DA and active damping control

The numerical evaluation of Figure 3.18 was verified experimentally using the setup of Figure 3.19. One additional accelerometer was added to the PMA‟s mass and used in evaluating the relative velocity of the mass with respect to the structure. Note that the relative acceleration was measured and integrated to realize the relative velocity. The block diagram of the cascade of controllers is shown in Figure 3.20 and the experimentally evaluated FRFs are presented in Figure 3.21.

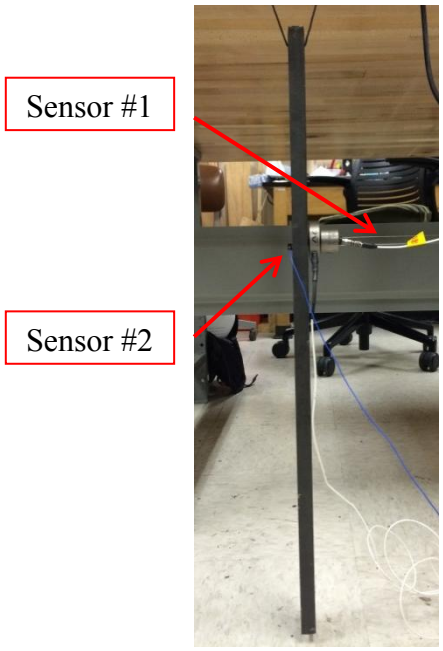

Figure 3.19: Experimental setup of the active damping

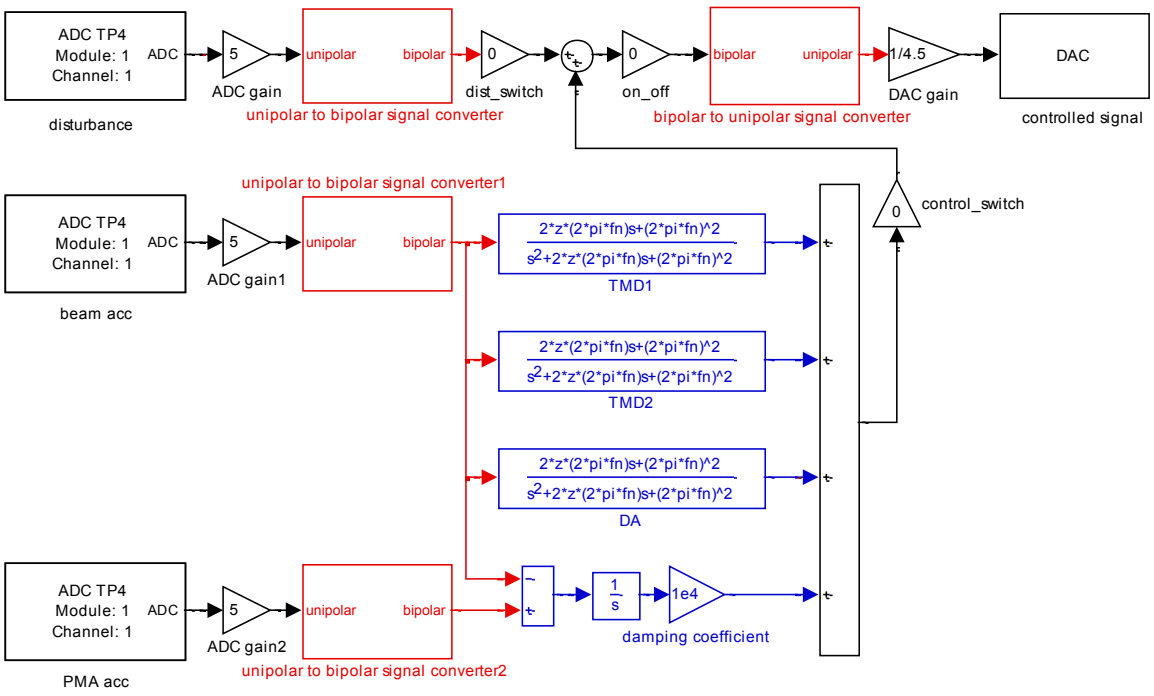

Figure 3.20: TMD_DA and active damping control interface

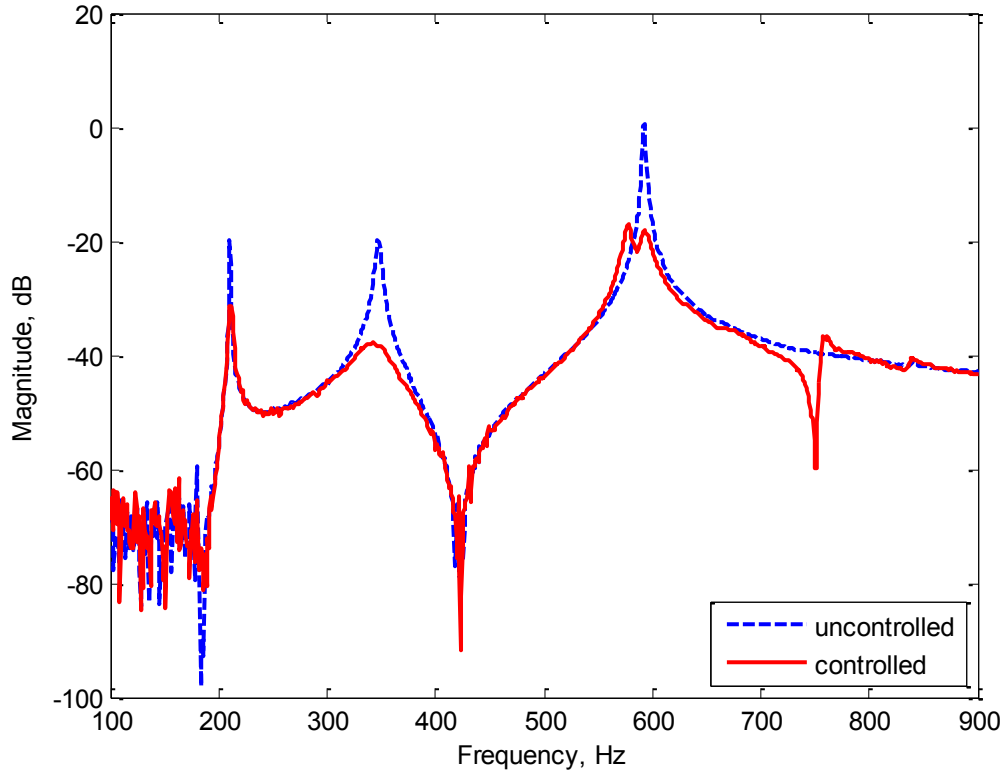

Figure 3.21: Experimentally measured FRF mapping the perturbation input to the acceleration without (blue trace) and with (red trace) TMD_DA and active damping control

Clear from Figure 3.21, damping of the PMA, tuned damping of two of the structure"s modes, and absorption at a forcing frequency have all been achieved, simultaneously.

The advantages of the TMD and DA control schemes are being simple and yet very effective in vibration reduction.

3.9 Linear Quadratic Gaussian (LQG) Control Scheme

As stated earlier the alternative to setting the natural frequency of the PMA substantially lower than the lowest natural frequency of the structure targeted for damping, is placing the natural frequency of the PMA a) to that of the structure if only one mode needs to be damped or b) within the frequency range of interest if damping of multiple modes is sought. This design strategy results in a proof mass actuator with a resonance in the frequency range where the active system needs to be most effective. On the positive side, this strategy put less demand on the actuator in term of providing actuation. On the negative side, this strategy requires controllers that are somewhat more involved/elaborate than the first control scheme. An example of such controllers is the estimator-based Linear Quadratic Gaussian (LQG) commonly used to achieve active multi resonance damping.

3.9.1 Controller Design

As stated earlier LQG is a full state-estimate feedback controller. The states are estimated by a Kalman estimator which uses the control force as well as the measurement error (the difference between the measured and estimated output, i.e., acceleration) as the inputs.

The state space formulation of the Kalman estimator is shown by Equation (3.22) and (3.23) where y , $\hat{y}$, L and u represent the measured acceleration, estimated acceleration, Kalman filter gain and control force, respectively.

$$\dot{x} = \hat{A}\hat{x} + \hat{B}u + L(y - \hat{y}) \tag{3.22}$$

$$\hat{y} = \hat{C}\hat{x} + \hat{D}u \tag{3.23}$$

The control force is the linear combination of states, i.e.,

$$u = -K\hat{x} \tag{3.24}$$

where K is evaluated by solving the algebraic Riccati Equation.

In order to obtain the state space formulation needed in the right format, the steps shown by Equations (3.25) through (3.28) are taken.

Substitute for u in Equation (3.23) from Equation (3.24)

$$\hat{y} = \hat{C}\hat{x} - \hat{D}K\hat{x} = (\hat{C} - \hat{D}K)\hat{x} \tag{3.25}$$

Substitute for u in Equation (3.22) from Equation (3.24)

$$\dot{\hat{x}} = \hat{A}\hat{x} + \hat{B}(-K\hat{x}) + L[y - (\hat{C} - \hat{D}K)\hat{x}] \tag{3.26}$$

$$\dot{x} = [\hat{A} - (\hat{B} - L\hat{D})K - L\hat{C}]\hat{x} + Ly \tag{3.27}$$

From Equation (3.24) and (3.27), the new state space formulation of the LQG regulator can be obtained shown by Equation (3.28). Note that D_{LQG} is zero.

$$\begin{aligned} \dot{\hat{x}} &= \underbrace{[\hat{A} - (\hat{B} - L\hat{D})K - LC]}_{A_{LQG}}\hat{x} + \underset{B_{LQG}}{\begin{matrix} L & y \end{matrix}} \\ u &= \underset{C_{LQG}}{\begin{matrix} -K \end{matrix}}\ \hat{x} \end{aligned} \tag{3.28}$$

3.9.2 LQG Vibration Control

The model of the plant (beam plus PMA), Equation (3.18), derived in the TMD_DA control approach and the experimental setup shown in Figure 3.1 were used to implement the LQG active damping control. The goal of the experiment was dampening multiple modes of the beam (with free-free boundary conditions), in the frequency range

of 100 to 900Hz, using the piezoelectric PMA with its natural frequency placed within the above-mentioned frequency range.

Figure 3.22 shows the FRFs of the beam measured at the accelerometer location, without and with the LQG based active damping control. A piezoelectric PMA with the natural frequency of 340Hz was used for both perturbation and control actuation. Clear from this figure, the LQG control scheme added damping to all the resonances of the structure (the beam) in the frequency range of interest. Note that the resonance at 340Hz belongs to the PMA itself, not the structure.

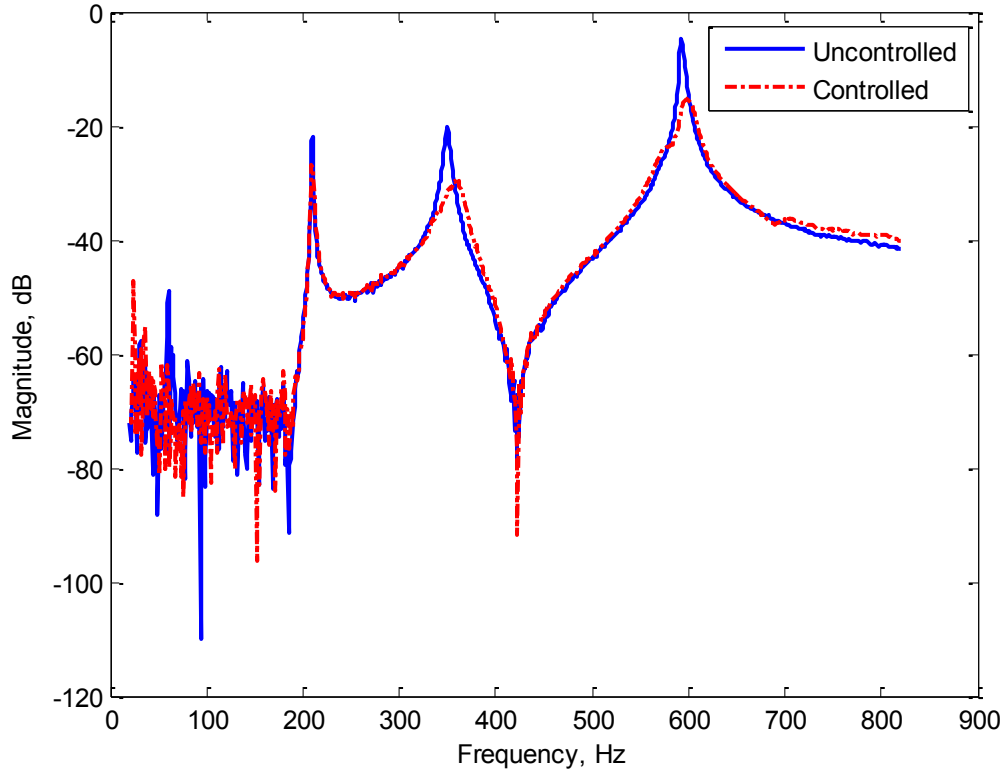

Figure 3.22: Experimentally measured FRF mapping the perturbation input to the acceleration without (blue trace) and with (red trace) LQG control

3.10 LQG Control plus TMD Control plus DA Control

As shown in Figure 3.22 the effectiveness obtained using LQG control compared to the result shown in Figure 3.21 by TMD + DA control, is somewhat limited. To enhance the damping effectiveness on the targeted (3rd) mode and also vibration absorption effectiveness at the perturbation frequency, a TMD controller and a DA controller were cascaded, in parallel, with the LQG controller. The TMD controller was tuned to the 3rd mode at 620Hz and the DA controller was tuned to the frequency of the disturbance at 750Hz. The Experimentally measured FRF mapping the perturbation input to the acceleration without (blue trace) and with (red trace) LQG control plus TMD + DA control are shown in Figure 3.23.

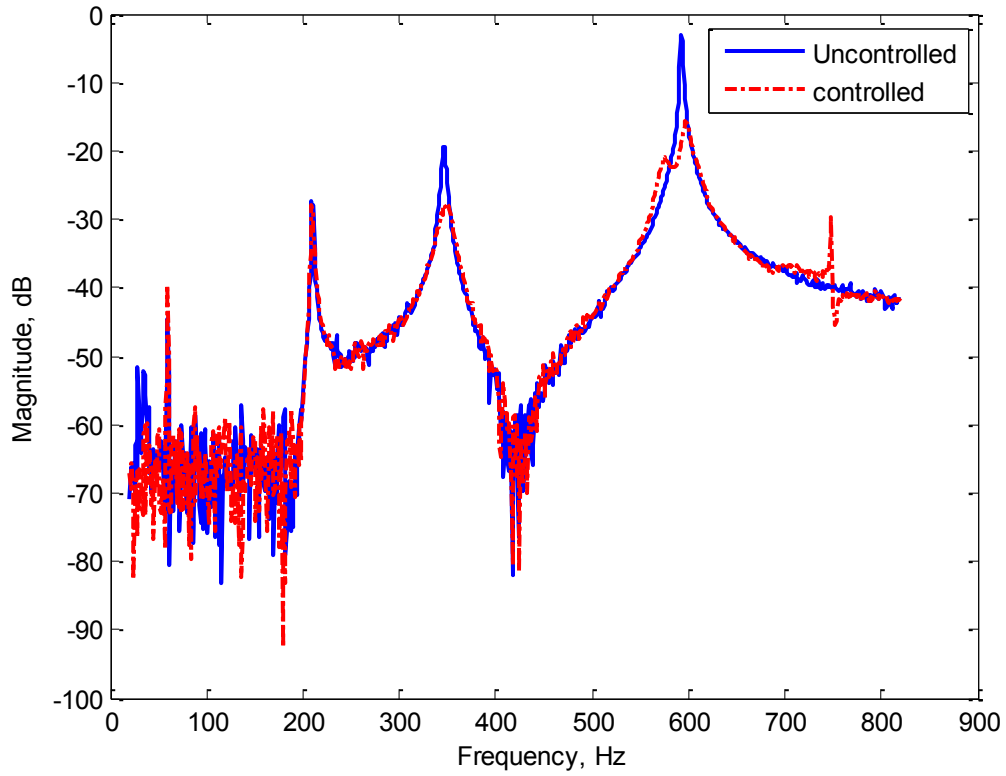

Figure 3.23: Experimentally measured FRF mapping the perturbation input to the acceleration without (blue trace) and with (red trace) LQG control plus TMD_DA control

Clear from Figure 3.23, the DA located at 750Hz can successfully absorb the vibration caused by the perturbation coming from outside. On the negative side, this cascaded control scheme spilled some energy into the 1st mode. Fortunately, the 1st mode is not in the frequency range of interest in this project, i.e., the test vehicle does not have the noise issue around the frequency of the 1st mode.

Each of the two control schemes presented in this document has its own advantages and disadvantages. Many factors need to be considered in choosing the right control scheme including power consumption, complexity, reliability, cost and so on. Moreover using multiple control schemes together can be a viable option. Cascading the LQG controller with TMD + DA controller has introduced more damping and absorption to the target mode and at the perturbation frequency.

3.11 Rear Axle Control

To examine the effectiveness of active vibration control on a real vehicle axle, an old solid rear axle was used as the structure. Considering the high rigidity of solid axles, our existing piezoelectric PMAs were not large enough to have sizable actuation. A regular (non-proof mas) actuator (of magnetostrictive type) was used to perturb and control the structure.

Figure 3.24 shows experimental setup of the solid axle with the regular actuator installed on (a) and measured FRF of the rear axle (equipped with the regular actuator) with the control off and on (b). An active dynamic absorption algorithm tuned to the frequency of 534Hz was used as the controller. The notch in the FRF of Figure 3.24(b) at

the tuning frequency shows the viability of active vibration control on such massive structure.

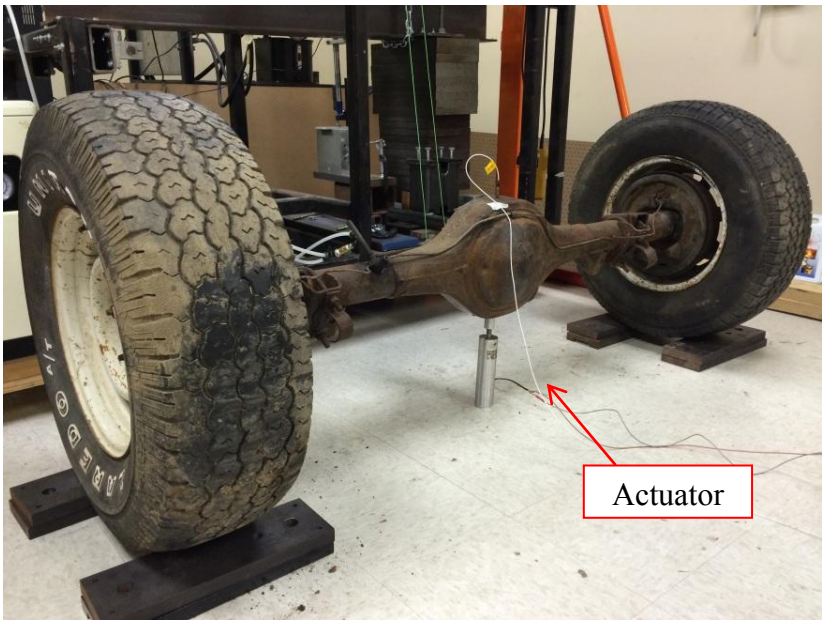

(a)

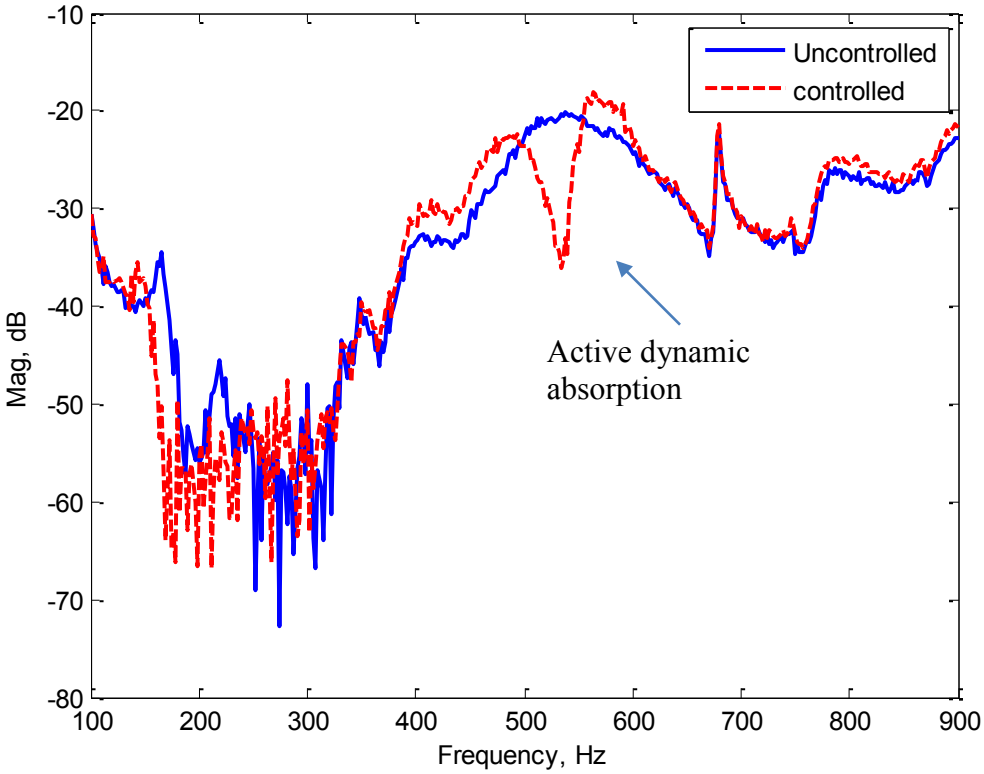

(b)

Figure 3.24: The experimental set up with the regular actuator (a) and measured FRF of the rear differential equipped with the regular actuator with the control off and on (b)

CHAPTER IV

TEST VEHICLE EVALUATION

4.1 Active Vibration Control Implementation

Following the laboratory work in developing the vibration control strategies using proof mass actuators, the first vibration control scheme mentioned earlier was chosen as the controller candidate for implementing on the vehicle. The choice was based on the baseline measurements of the rear axle of the candidate vehicle exhibiting whine noise at around 450Hz corresponding to the vehicle speed of 93km/hr.

In the initial attempt, two piezoelectric proof mass actuators with 150 gram mass were used for actuation. The natural frequencies of the PMAs were set below the 450HZ frequency of interest (critical frequency). Figure 4.1 shows an image of the actuator installed on the rear subframe.

Figure 4.1: One of the two piezoelectric PMAs installed on the rear subframe

Although the piezoelectric PMAs exhibited effectiveness in mitigating 450Hz vibration in shaker tests, but the test on the dynamometer with constant speed at the critical frequency showed the lack of effectiveness of these actuators in absorbing the vibration induced by the rear differential.

The piezoelectric proof mass actuators were replaced with two larger, 18 watt (at 20 deg C), electromagnetic proof mass actuators with 250 gram inertial masses. Figure 4.2 shows the FRF mapping the voltage to the force output of these actuators, measured in the laboratory. The rather large inductors in these actuators which along with a strong magnet produce large forces, also introduces up to 90 degrees of phase lag, at high frequencies (well beyond their resonant frequency), into the dynamics of the electromagnetic PMAs.

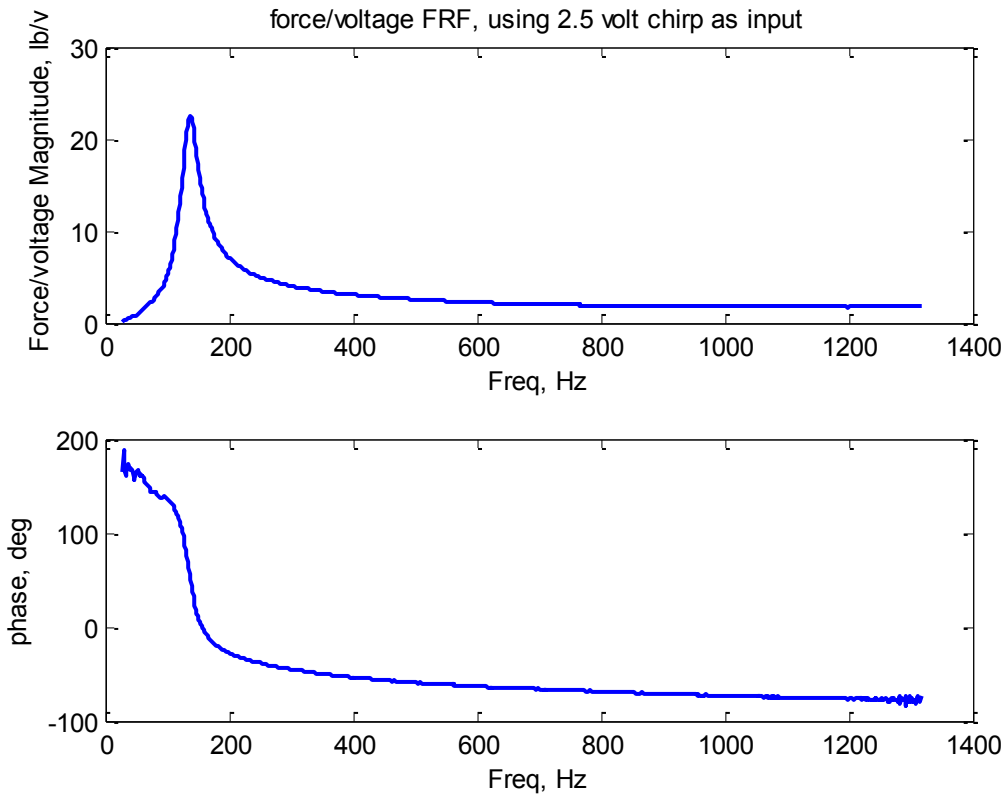

Figure 4.2: FRF of electromagnetic PMA

First the electromagnetic PMAs were installed at the same locations as those of the piezoelectric actuators shown in Figure 4.1 and later moved to their new location underneath the front bushings attaching the rear differential to the subframe as it is shown in Figure 4.3. An accelerometer nearly-collocated with each actuator, provided the sensory information to the controller.

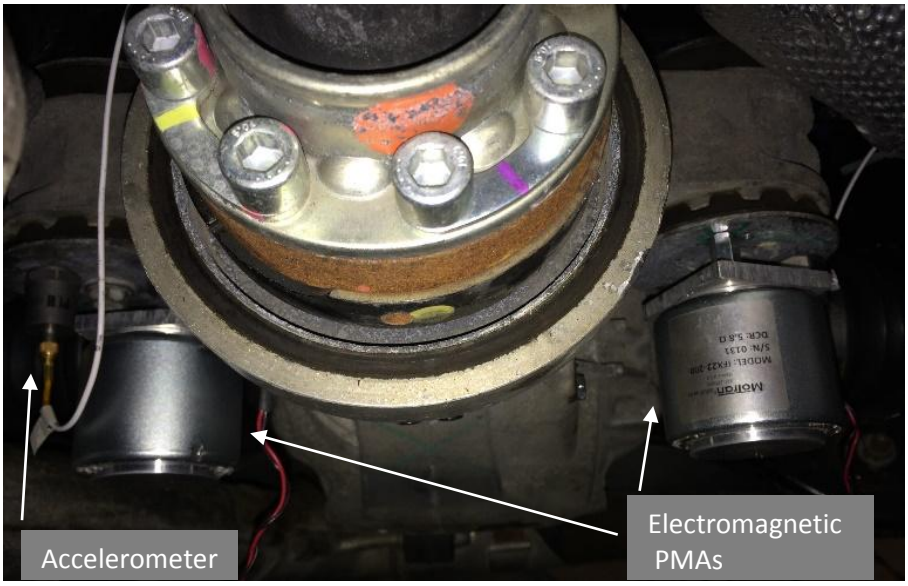

Figure 4.3: Location of the electromagnetic PMA on the subframe

The availability of space to house the actuators, somewhat a) on the transfer path of the vibration and b) as close as possible to the source of vibration i.e., the rear drive shaft and differential were the main deciding factors on the placement locations of the actuators.

To investigate the dynamics of the rear drive shaft/differential and the subframe an additional electromagnetic PMA was installed, temporarily, on the drive shaft and used as a shaker. To perturb the drive shaft both in torsion and bending, the shaker was installed off-center on the drive shaft shown in Figure 4.4. To avoid the gear and u joint backlash introducing nonlinearities during the shaking test, the vehicle was placed/parked on a ramp.

Figure 4.4: Shaker placement on the rear drive shaft

4.2 Rear Subframe Active Vibration Control

The presence of no prominent resonance around the frequency of interest, ruled out the need for adding active tuned damping to the subframe. To lower the transmission of forced vibration at the frequency of interest from the rear differential to the vehicle, the use of an active vibration absorption strategy was decided on.

Using the acceleration measured by the feedback sensor on the front bushing of the rear subframe, the FRFs mapping the voltage driving the shaker (installed on the drive shaft) to the aforementioned accelerations were measured. Figure 4.5 shows the magnitude of these FRFs with the control loop open (blue/solid line traces) and closed (red/dashed line traces). The placement of a zero (a notch) at the frequency of interest on the FRF magnitude indicates the effectiveness of the active vibration control scheme in absorbing vibration at the frequency of interest, i.e. the perturbation frequency.

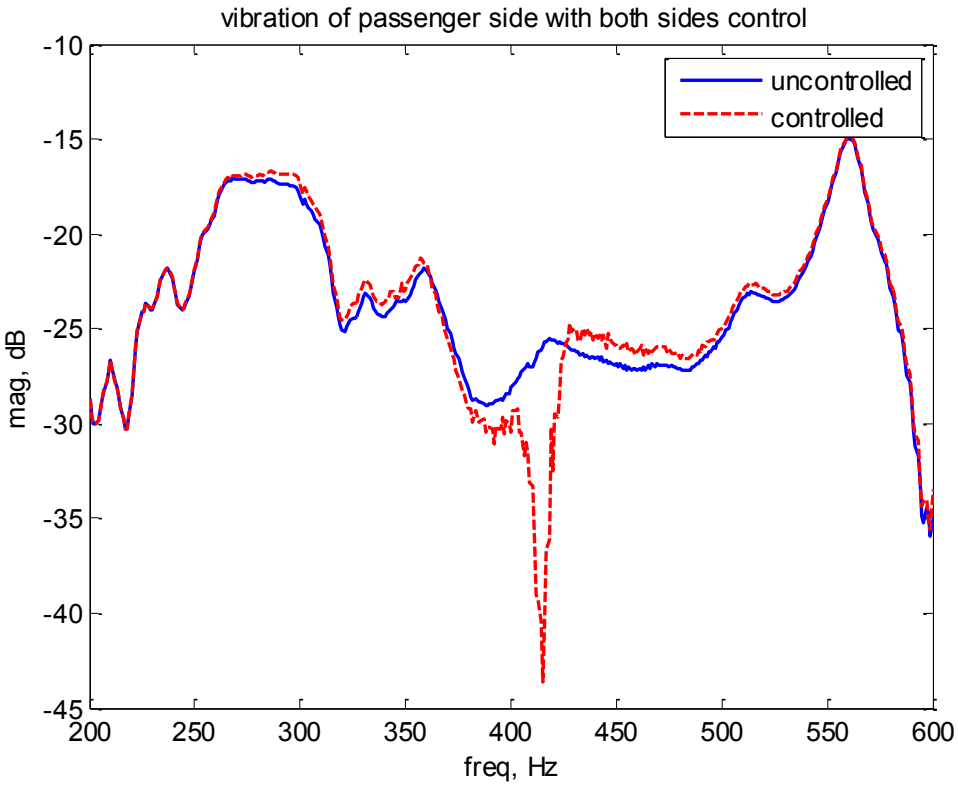
vibration of passenger side with both sides control
uncontrolled
controlled
mag, dB
freq, Hz
-10
-15
-20
-25
-30
-35
-40
-45
200
250
300
350
400
450
500
550
600

(a)

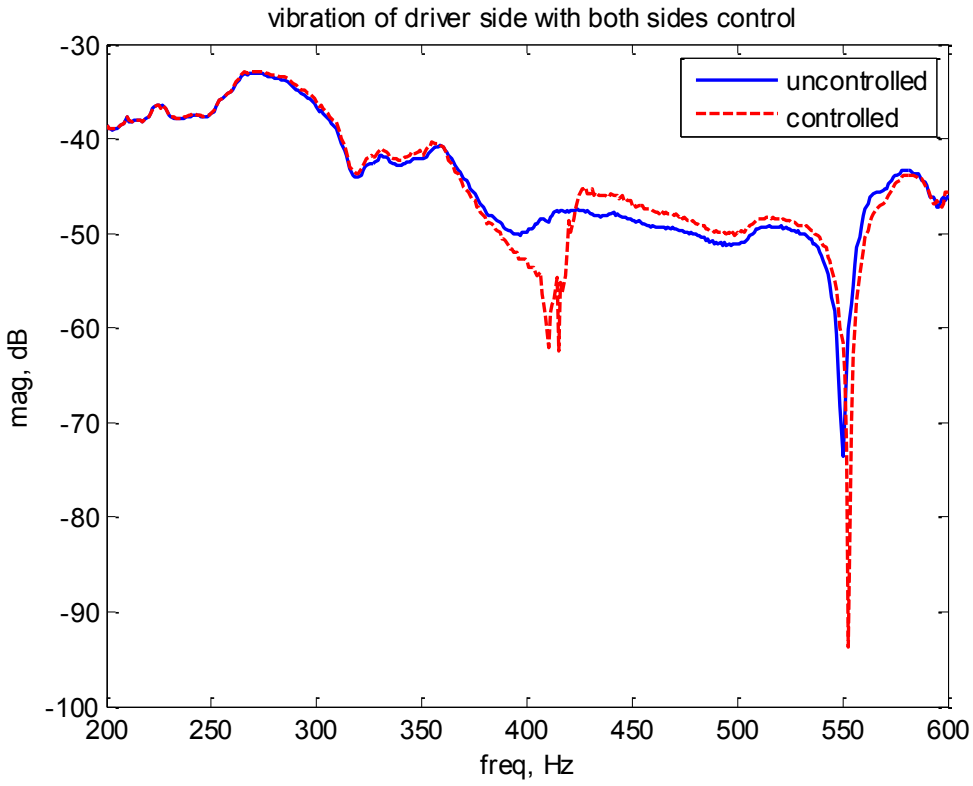

(b)

Figure 4.5: FRFs of acceleration of the passenger side subframe bushings (a) and driver side subframe bushings (b) with the voltage driving the driver shaft shaker as the input

The evaluation of the control scheme continued by perturbing the drive shaft (by the shaker) with a tonal perturbation at the tuning frequency of the DA controller and measuring pressure in the cabin by a microphone placed close to the driver's ear. Figure 4.6 shows the power spectra of such measurement without and with the control loops closed. The comparison of the power spectra in Figure 4.6 indicates the effectiveness of the control scheme in lowering the tonal noise.

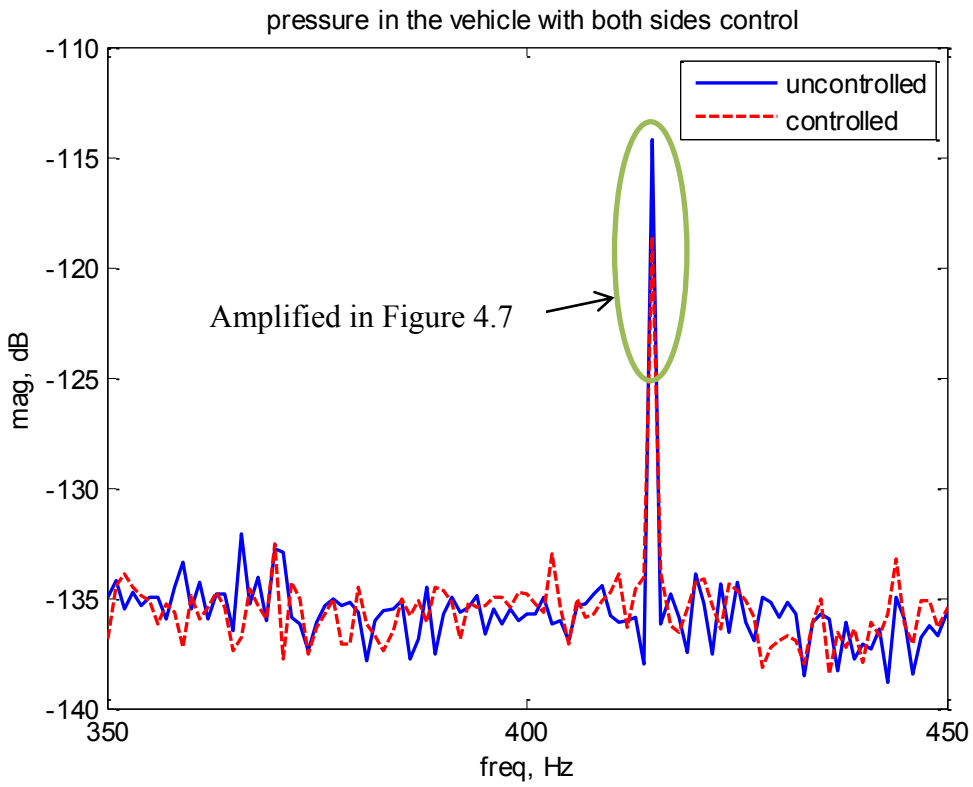

Figure 4.6: Power spectra of pressure next to the driver's ear, with the active vibration control off (blue trace) and on (red trace), measuring during the shaker test

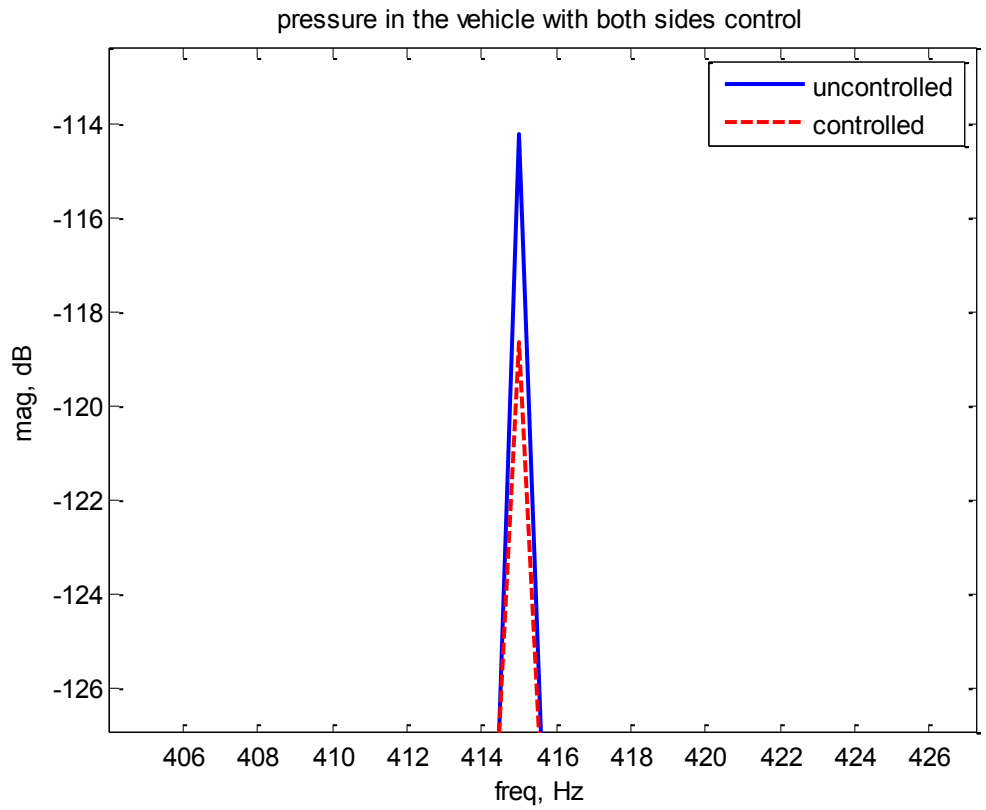

Figure 4.7: Amplified area with ellipse in Figure 4.6

Following the shaker test, the perturbation actuator was removed from the drive shaft and the vehicle with the control hardware installed on its rear subframe, was placed on the rolling dynamometer and tested at the constant speed of 93km/hr, as shown in Figure 4.8. To prevent the vehicle from down shifting, the torque load was limited to below 54 Nm (40 ft lb).

Figure 4.8: The vehicle on rolling dynamometer

With the vehicle running on the constant speed of 93km/hr, the accelerations on the front bushings of the rear subframe as well as the pressure next to driver's ear were measured with the active vibration control scheme being off and on. Figure 4.9 compares the power spectra of aforementioned accelerations, showing the absorption of vibration at the target frequency.

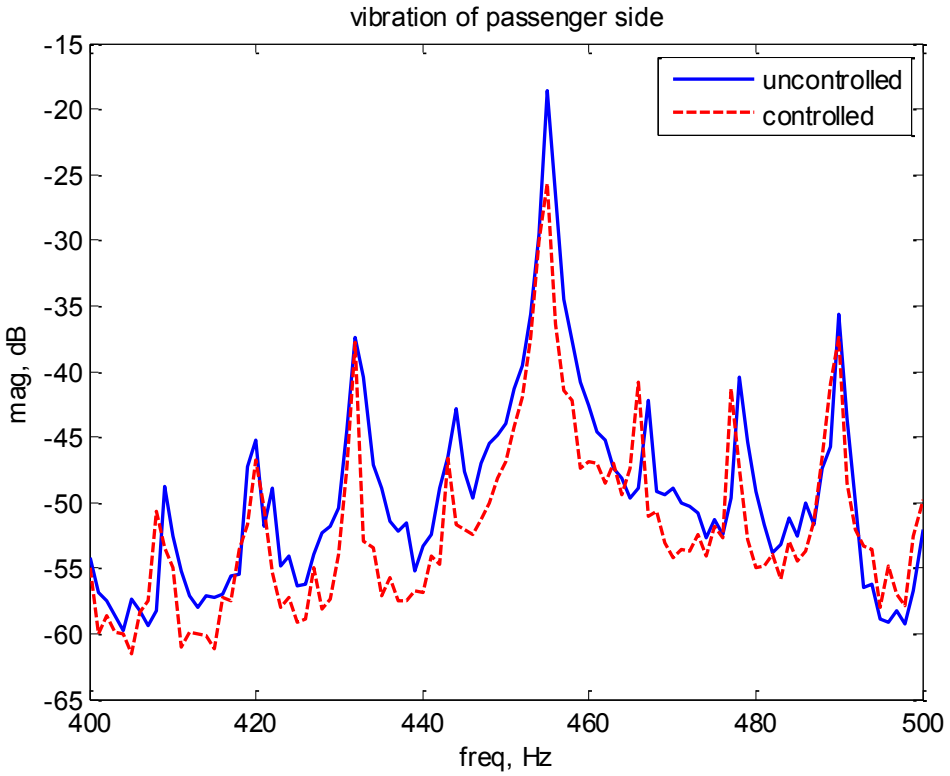
vibration of passenger side
uncontrolled
controlled
mag, dB
freq, Hz
-15
-20
-25
-30
-35
-40
-45
-50
-55
-60
-65
400
420
440
460
480
500

(a)

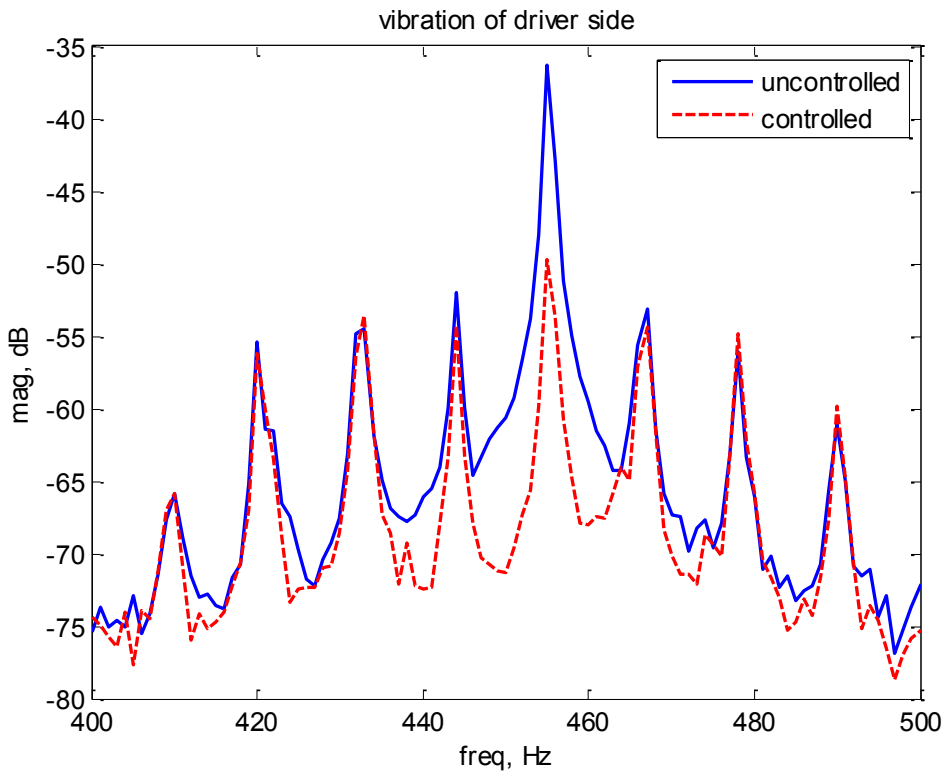

(b)

Figure 4.9: Power spectra of the measured acceleration of the passenger side subframe bushing (a) and driver side subframe bushing (b) with the active vibration control off (blue trace) and on (red trace), measured during the rolling dynamometer test

Figure 4.10 compares the power spectra of pressure measured next to the driver's ear, with the active vibration control off and on. The comparison of the traces points to the abatement of noise at the target frequency.

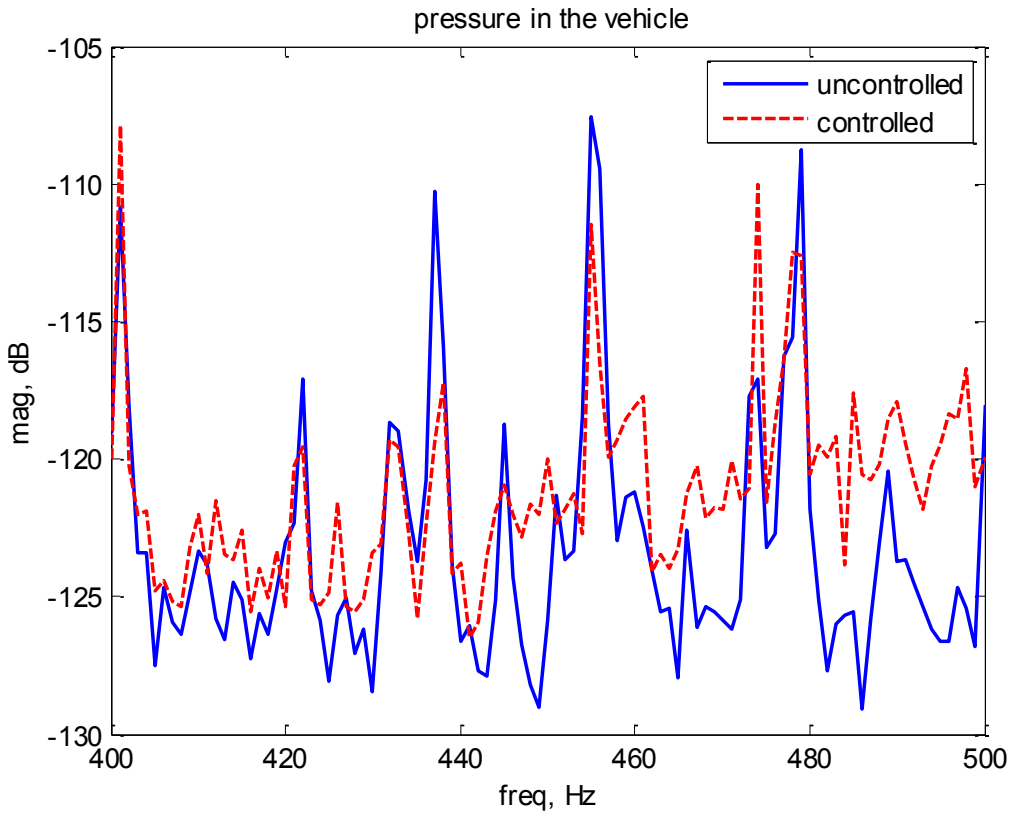

Figure 4.10: Power spectra of pressure next to the driver's ear, with the active vibration control off (blue trace) and on (red trace), measured during the rolling dynamometer test

CHAPTER V

SUMMARY

5.1 Conclusion

In the field of active vibration control, PMA has been widely used to suppress the vibration caused by the external excitation. Unlike regular actuators, PMAs do not need anchors to push against; PMAs are not effective at low frequencies but are highly effective at high frequencies.

Based on the FRF mapping the voltage of the active element to the force generated by PMA, several control strategies can be applied depends on the frequency range of interest. Two of the control strategies are designed and evaluated numerically and experimentally. The effectiveness of active control in absorbing the shaker induced vibration of rear subframe of a test vehicle was successfully demonstrated by examining the extent of reduction in the vibration of the rear subframe as well as the sound pressure inside the vehicle. Moreover, rolling dynamometer tests have shown effectiveness of the active control in reducing the vibration of the rear subframe and the pressure inside the cabin caused by the rear differential gear mesh.

5.2 Future Work and Recommendation

The experimental results on the test vehicle show the success of the TMD/DA control schemes developed in the laboratory. However, more work can be done to mature this technology. The following are the recommendations:

1. Extending the single frequency control to multifrequency control.
2. Introducing adaptability into the controller by following the speed of the drive shaft.
3. Extending the one directional control to multidirectional control.
4. Exploring the model-based control application.

REFERENCES

[1] Bohna, C. Cortabarriaa, A. Hartela, V. Kowalczyk, K. "Active control of engine-induced vibrations in automotive vehicles using disturbance observer gain scheduling" Control Engineering Practice 12 (2004) 1029–1039

[2] Eulert, S., Luhrs, G., Brraunig, J., Bucht, A. and Kunze, H. "Reduction of the inner vehicle noise level by active vibration damping of the rear axle drive" VDI-Berichte Nr. 218, 2011

[3] Vajreshwari Umachagi, Katta Venkataramana, G. R. Reddy, Rajeev Verma. "Applications of Dampers for Vibration Control of Structures: an Overview", IC-RICE Conference Issue, Nov-2013

[4] ANTHONY C. WEBSTER and RIMAS VAICAITIS, "Application of Tuned Mass Dampers to Control Vibrations of Composite Floor Systems", American Institute of Steel Construction, Inc, 2003

[5] Jeffrey J. Dosch, Daniel J. Inman and Ephrahim Garcia, "A Self-Sensing Piezoelectric Actuator for Collocated Control", Journal of Intelligent Material Systems and Structures 1992 3: 166

[6] Cristóbal González Díaz, Christoph Paulitsch, and Paolo Gardonio, "Active damping control unit using a small scale proof mass electrodynamic actuator", J. Acoust. Soc. Am., Vol. 124, No. 2, August 2008

[7] Nishimura, I. Kobori, T. Sakamoto, M. Koshika, N. Sasaki, K. and Ohrui, S " Active Tuned Mass Damper," Smart Mater. Struct. 1 (1992) 306-311.

[8] Kirk D. "Optimal Control Theory: An Introduction" Courier Dover Publications, 2012

[9] Chin-Hsiung Loh and Pay-Yang Lin, "Kalman Filter Approach for the Control of Seismic-Induced Building Vibration Using Active Mass Damper Systems", The Structural Design of Tall Building, Vol. 6, 209-224 (1997)

APPENDICES

A. TMD and DA Controller Design

Figure A - 1 shows the schematic diagram of a passive control scheme (namely a TMD) appended to a structure. m_1, k_1, c_1 are the parameters (mass, stiffness and damping coefficient) of the structure, m_2, k_2, c_2 are the parameters of the controller, and x_1, x_2 are the displacement of the structure and controller mass, respectively.

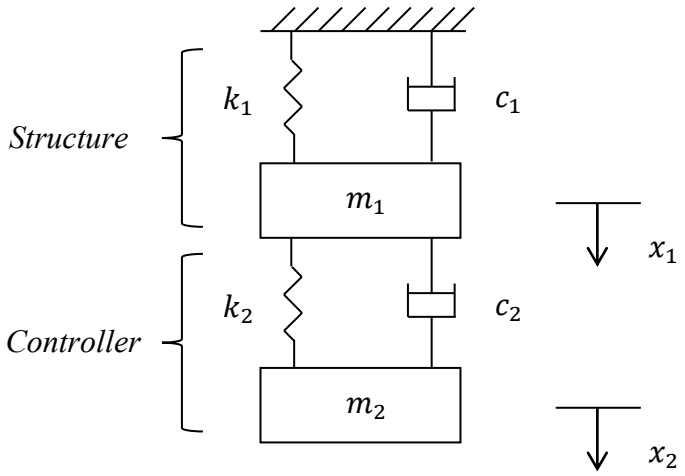

Figure A - 1: Schematic diagram of the control algorithm

The structure is subject to a disturbance which causes vibration of the structure marked by displacement x_1. The vibration of the structure will be transmitted to the

spring-mass-damper system named controller, resulting in vibration of mass m_2 marked by displacement x_2. Equation (A-1) shows the transfer function of the controller with the displacement of the structure, where the controller is appended to, as the input and the displacement of the controller as the output.

$$\frac{x_2}{x_1} = \frac{c_2 s + k_2}{m_2 s^2 + c_2 s + k_2} \tag{A-1}$$

Changing the relationship of displacement between the structure and the controller to acceleration results in Equation (A-2).

$$\frac{x_2}{x_1} = \frac{a_2 s^2}{a_1 s^2} = \frac{a_2}{a_1} = \frac{c_2 s + k_2}{m_2 s^2 + c_2 s + k_2} \tag{A-2}$$

where a_1 and a_2 are the acceleration of the structure and the controller respectively.

The acceleration of the controller multiply its mass generates a control force exerted on the structure. Equation (A-3) shows the transfer function of the controller, describing the acceleration of the structure as the input with the control force as the output.

$$\frac{a_2}{a_1} = \frac{a_2 m_2}{a_1} = \frac{f}{a_1} = \frac{(c_2 s + k_2) m_2}{m_2 s^2 + c_2 s + k_2} \tag{A-3}$$

where f is the force produced by the controller.

Dividing both numerator and denominator of Equation (A-3) by m_2 yields another transfer function format of the controller shown in Equation (A-4).

$$\frac{f}{a_1} = m_2 \frac{2\xi_2 w_{n2} s + w_{n2}^2}{s^2 + 2\xi_2 w_{n2} s + w_{n2}^2} \tag{A-4}$$

where ζ_2 and w_{n2} are the damping ratio and natural frequency of the controller. Depending on the extent of damping ζ_2, the passive controller is either a TMD or a DA.

The transfer function of the controller presented by Equation (A-4) can be used as an active vibration controller either as the TMD controller or the DA controller. Note that the difference between these two controllers is the damping ratio. Normally the TMD controller has a large damping ratio whereas the damping ratio is small in DA controller. In addition, the TMD controller is used to target the modes of the structure but DA controller is used to absorb forced vibration which depends on the forcing frequency.

B. Active Vibration Control Schemes Comparison

In Chapter III, the TMD controller is introduced to add damping to the resonant frequencies of the structure. However, another active vibration control scheme dubbed as ATMD controller can achieve the same effectiveness by feeding back the acceleration of the target mode. The feedback gain is derived using the dynamics of passive TMD.

To explore the advantages and disadvantages of these two control schemes, a 4-mode structure with 1% damping is created in simulation. The natural frequencies of the first two modes of the structure are 0.3473rad/sec and 1rad/sec respectively. The PMA is tuned to the first mode of the structure and the TMD controller as well as the ATMD controller is used to control the second mode of the structure in comparison. Also, the ATMD controller is added to the first mode in both scenarios. The schematic block diagram of the two control schemes are shown in Figure B - 1.

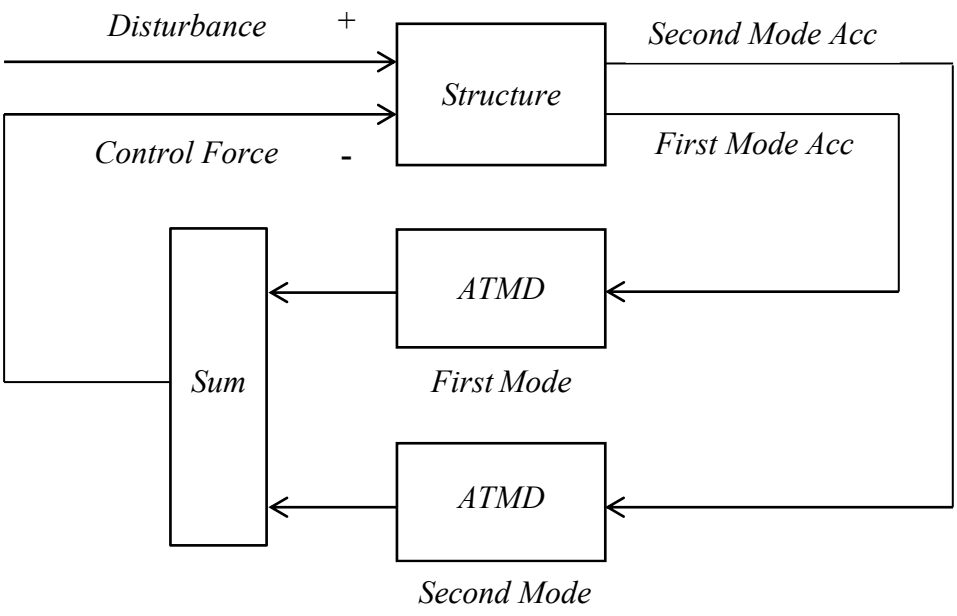

(a)

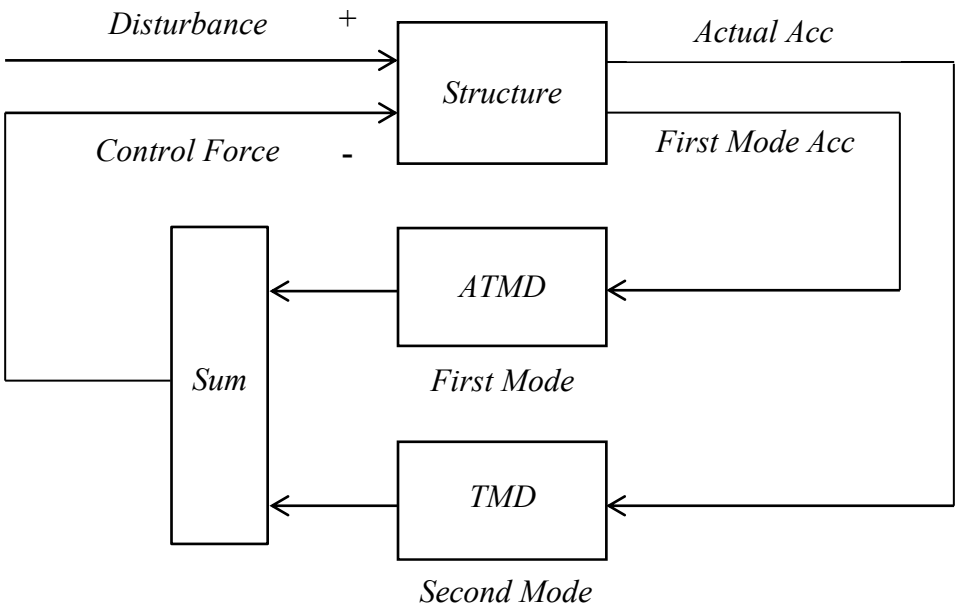

(b)

Figure B - 1: Schematic block diagram of the ATMD control (a) and TMD control (b)

Note that the ATMD controller needs the modal acceleration to be the feedback signal while the physical measured acceleration is used in the TMD controller. Mode shapes (eigenvectors) of the structure and additional sensors are needed to get the measurement result of the modal acceleration.

In order to compare the performance of the two control schemes, such as the stroke and power consumption of the PMA, the two controllers are adjusted to have almost the same effectiveness on the 2^{nd} mode and an impulse disturbance is used to perturb the system. It is found that there is not much difference between these two control strategies in stroke, power consumption and so on. So based on the easier signal measurement, the TMD control scheme should be the better choice for this application.

Figure B - 2 shows the FRFs mapping the perturbation input to the displacement of the structure without and with the two control schemes.

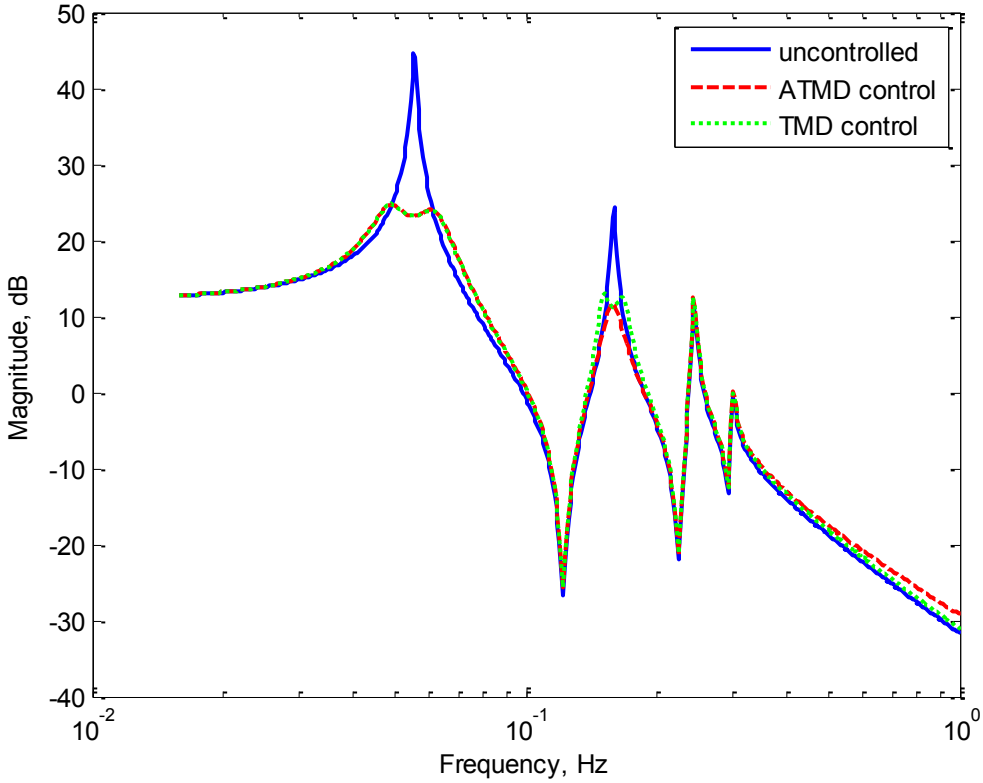

Figure B - 2: FRF mapping the perturbation input to the displacement without (solid trace), with ATMD (dashed trace) and with TMD (dotted trace) control